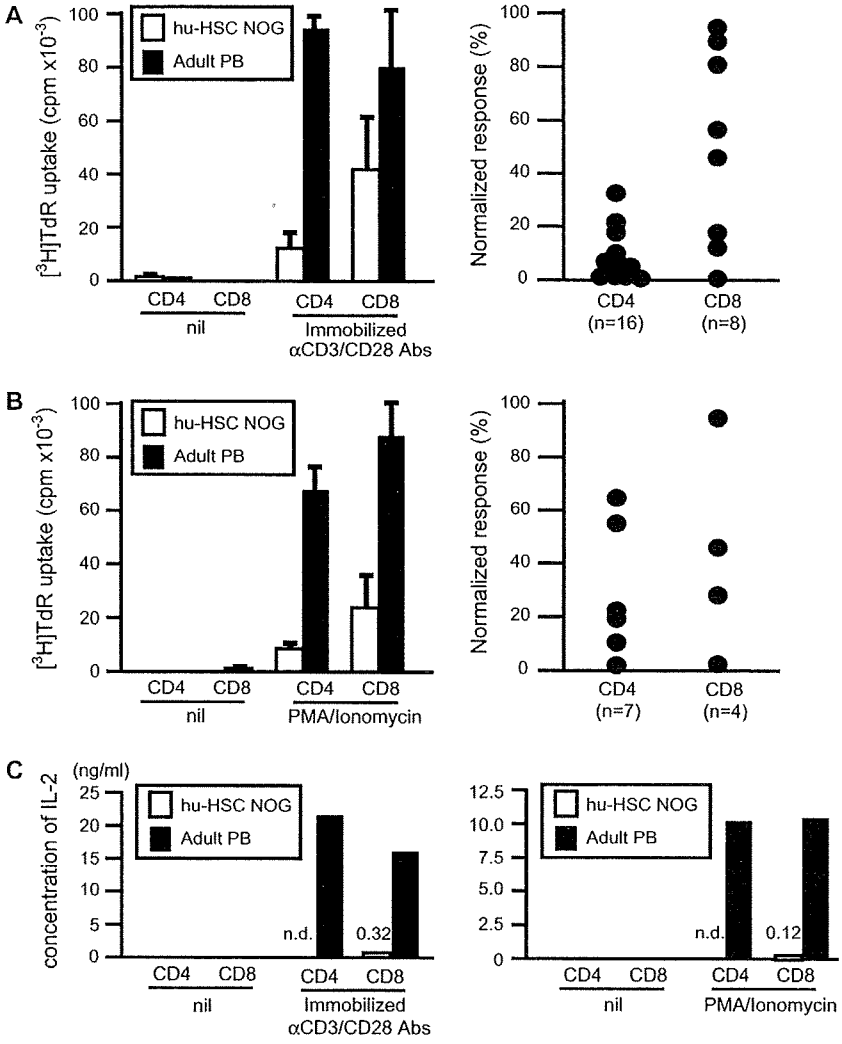

Fig. 6. Impaired responses of human T cells in hu-HSC NOG mice to mitogens. (A and B) Analysis of functions of human $CD4^+$ or $CD8^+$ T cells in hu-HSC NOG mice *in vitro*. $CD4^+$ or $CD8^+$ T cells were prepared from the spleen of the hu-HSC NOG mice (20 weeks after reconstitution) (white bar) or normal adult peripheral blood (PB) (black bar) as described in Methods. They were stimulated with immobilized anti-CD3 and anti-CD28 antibodies (A, left panel, $n = 16$ or 8 for $CD4^+$ T cells or $CD8^+$ T cells, respectively) or combination of PMA and ionomycin (B, left panel, $n = 7$ or 4 for $CD4^+$ T cells or $CD8^+$ T cells, respectively). After 72-h culture, the proliferation of T cells was measured as the amounts of incorporated [^{3}H]thymidine ([^{3}H]TdR) as in Fig. 5(C). The cumulative data are shown after normalizing the magnitude of the response of hu-HSC NOG T cells to that of PB T cells (right panels). (C) Quantification of IL-2 produced by human T cells in hu-HSC NOG mice *in vitro*. The amount of IL-2 in the supernatants obtained from the *in vitro* cultures described in (A and B) was measured by ELISA. n.d.: under detection level by ELISA.

Development of human T cells in NOG I-Aβ$^{-/-}$ mice

The results with the $CD4^+CD8^-$ SP thymocytes suggested that there were regulatory mechanisms to induce tolerance to the human T cells in the mouse periphery. To examine the involvement of mouse MHC molecules, we used the NOG I-Aβ$^{-/-}$ strain. In these mice, we could not detect any mouse $CD4^+$ T cells, as previously reported. Upon humanization, surprisingly, human T cells could be detected in the spleen of the hu-HSC NOG I-Aβ$^{-/-}$ mice (Fig. 9A). Thus, the HLA class II molecules on the human T cells (38) or a quite small number of human B cells or human dendritic cells (DCs) in the thymus positively selected human T cells in the mouse thymus. Although we could not detect a significant number of $CD4^+CD8^-$ SP thymocytes in the hu-HSC NOG I-Aβ$^{-/-}$ mice by FACS analysis after 20 weeks of reconstitution (Fig. 9B), these $CD4^+$ T cells were not derived from extrathymic tissues because no human T cells appeared in hu-HSC NOG *nu/nu* mice (data not shown), suggesting that the mouse thymus was indispensable for the human T-cell development. The number of $CD4^+$ T cells in the spleen was <1% of that in the regular hu-HSC NOG mice at 16 weeks after reconstitution and reached 20% at ~20 weeks (4.9×10^5, $n = 15$, in the regular hu-HSC NOG versus 1.2×10^5, $n = 4$, in the hu-HSC NOG I-Aβ$^{-/-}$ NOG). It is uncertain whether this increase was caused by the homeostatic proliferation

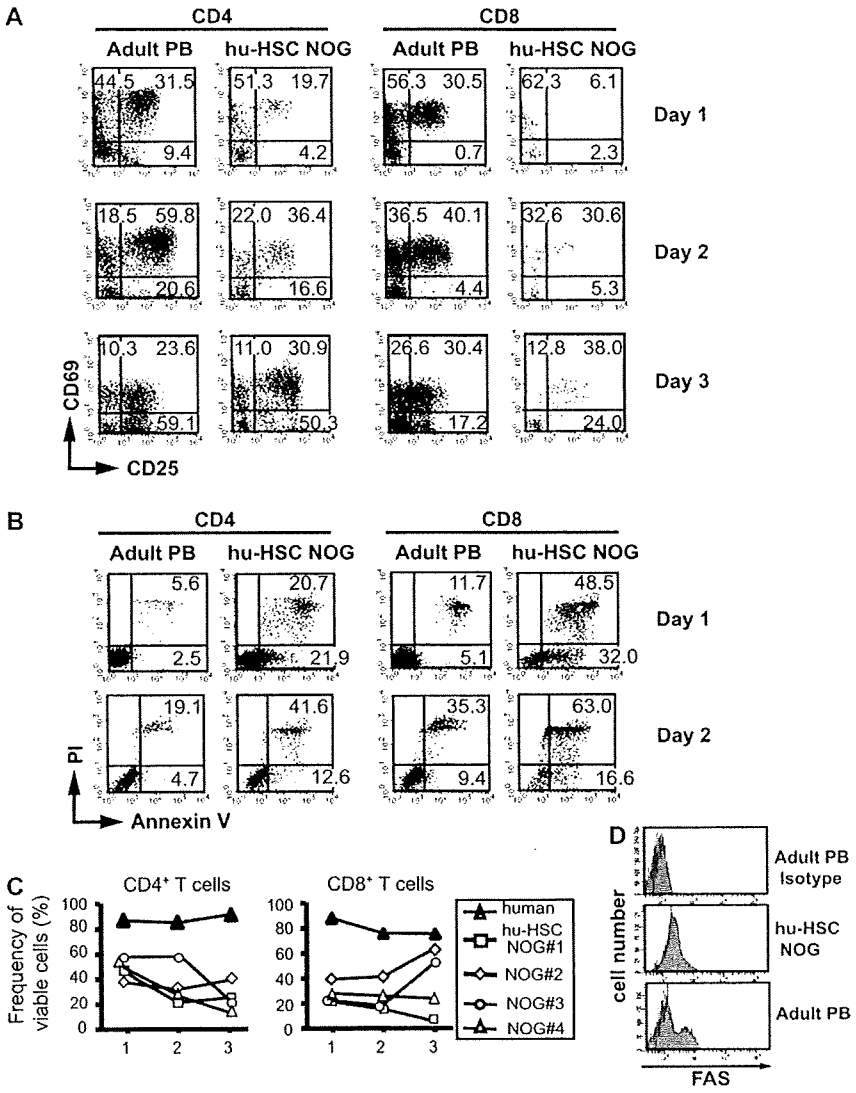

Fig. 7. Enhanced cell death of hu-HSC NOG T cells. (A) Analysis of activation markers of T cells. Purified $CD4^+$ or $CD8^+$ T cells from hu-HSC NOG mice (20 weeks after reconstitution) or human peripheral blood (PB) were stimulated by immobilized anti-CD3 and anti-CD28 antibodies as described in Fig. 6. The expression of CD25 and CD69 on them were analyzed every 24 h. A representative result from three independent animals is shown. (B) Analysis of apoptosis induced in T cells. The *in vitro* cultured $CD4^+$ or $CD8^+$ T cells as in (A) were stained with annexin V and PI at 24 and 48 h. A representative result from four independent experiments is shown. (C) Survival curve of *in vitro* cultured T cells. The frequency of viable $CD4^+$ or $CD8^+$ T cells was represented as the percentage of annexin V and PI double-negative cells in the FACS analysis mentioned in (B). (D) Expression analysis of CD95 (Fas) on T cells. A representative result of staining with anti-CD95 antibody is shown.

of peripheral T cells or the accumulation of migrated T cells from the thymus. Due to the low number of $CD4^+$ T cells in the hu-HSC NOG I-A$\beta^{-/-}$ mice that could be purified for *in vitro* experiments, we instead stimulated the whole-spleen cells from these mice with anti-CD3 and anti-CD28 antibodies *in vitro* after CFSE labeling to examine their responsiveness. The dilution of CFSE in the T-cell population was measured on days 4 and 6. The human T cells in the hu-HSC NOG I-A$\beta^{-/-}$ mice showed no significant proliferation (Fig. 9C). Thus, the human T cells that developed in the absence of I-A were also rendered unresponsive.

IgG response in hu-HSC NOG mice upon the adoptive transfer of normal T cells

Our analyses revealed that the hu-HSC NOG mice have problems in both their B-cell and T-cell populations. However, since the B cells could mount an IgG response, if not complete, to *in vitro* stimulation, we next examined whether antigen-specific IgG responses were possible *in vivo*, if supplemented with functional T cells. For this purpose, we used a TCR specific for an HA peptide ($HA_{307-319}$) that was derived from an HA-specific human T-cell clone, B16 (31). The TCR was introduced into human T cells isolated from PBMCs by retroviral vectors (Fig. 10A). The expression of the

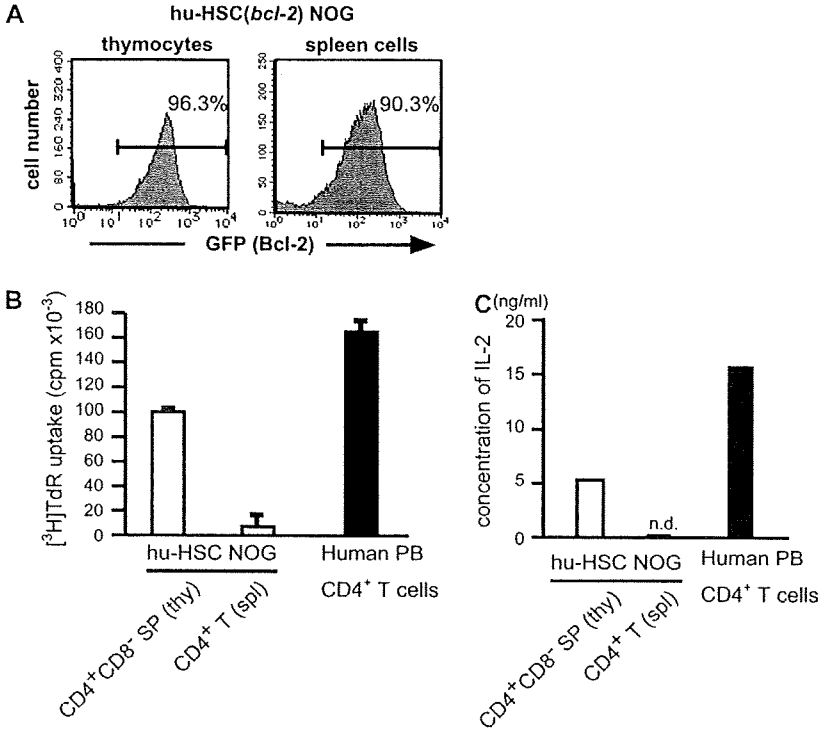

Fig. 8. Normal response of $CD4^+CD8^-$ SP thymocytes from hu-HSC NOG mice. (A) Reconstitution of hu-HSC (*bcl-2*) NOG mice. A representative analysis for expression of exogenous *bcl-2* represented by bicistronic GFP from retroviral vector in thymocytes and spleen cells. The thymocytes and spleen cells were prepared from the hu-HSC (*bcl-2*) NOG mice 20 weeks after reconstitution and examined the expression of GFP ($n = 6$). (B) Analysis of functions of human $CD4^+CD8^-$ SP thymocytes in hu-HSC (*bcl-2*) NOG mice *in vitro*. $CD4^+CD8^-$ SP thymocytes were prepared from pooled thymuses from five different hu-HSC (*bcl-2*) NOG mice grafted with the same $CD34^+$ cells (20 weeks after reconstitution). $CD4^+$ T cells were also purified from the same hu-HSC (*bcl-2*) NOG mice. These NOG-derived T cells (white bar) or normal adult peripheral blood (PB) (black bar) were stimulated with immobilized anti-CD3 and anti-CD28 antibodies. After 72-h culture, the proliferation of T cells was measured as the amounts of incorporated [^{3}H]thymidine ([^{3}H]TdR) as mentioned in Fig. 5(C). Representative data from three independent experiments are shown. (C) Quantification of IL-2 produced by human $CD4^+CD8^-$ SP thymocytes in hu-HSC (*bcl-2*) NOG mice *in vitro*. The amount of IL-2 in the supernatants obtained from the *in vitro* cultures described in (B) was measured by ELISA. n.d.: under detection level by ELISA.

antigen-specific TCR was also confirmed by staining with the specific tetramer (HLA-DRB1*0401/$HA_{307-319}$) (Fig. 10B). The transduced T cells produced IL-2 in response to the antigenic stimulation by a B-cell lymphoma cell line (*HLA-DRB1*0401* positive) loaded with the $HA_{307-319}$ peptide (Supplementary Figure S1, available at *International Immunology* Online). Because the B16 TCR is restricted by HLA-DR4 (DRB1*0401) and the frequency of this haplotype in the Japanese population is quite low (~1% of the population), the *HLA-DRB1*0401* gene was introduced into $CD34^+$ stem cells by retrovirus to obtain hu-HSC [HLA-DR4 (DRB1*0401)] NOG mice (Fig. 10C). We then transferred the human T cells containing the B16 TCR into the hu-HSC [HLA-DR4 (DRB1*0401)] NOG mice and immunized them with the $HA_{307-319}$ peptide (Fig. 10D). After repeating the transfer and subsequent antigenic challenges twice, we measured the amount of IgG specific for the HA peptide. Although the total IgG level in the sera was markedly elevated after immunization, the titer of HA peptide-specific IgG remained low (Fig. 10E). The increase in total IgG occurred through non-specific activation of the B-cell population by the B16 TCR-bearing human T cells, suggesting that the machinery for Ig class switch is also functional *in vivo*. We could not, however, detect any donor human T cells with the B16 TCR by staining with the specific tetramer (data not shown) 10 days after the final antigenic challenge, which may explain the absence of the HA-specific IgG response in the hu-HSC [HLA-DR4 (DRB1*0401)] NOG mice.

Discussion

In this study, we have clarified the possibilities and limitations of the present humanized mouse technology. The quasi-human immune system in humanized mice has been shown to be relatively similar to *bona fide* human immunity (5–9). However, the induction of successful immune reactions against exogenous antigens, especially the humoral responses represented by IgG responses, has been a high hurdle for humanized mice (21, 22, 24, 25). Several mechanisms have been suggested for this defect, including the skewing of human B cells toward the B-1 cell lineage (24), and the lack of interactions between B and T cells due to mismatches of the MHC (24). Our results suggest that in addition to these possibilities, other previously unrecognized mechanisms involving both B and T cells are also responsible for this limitation.

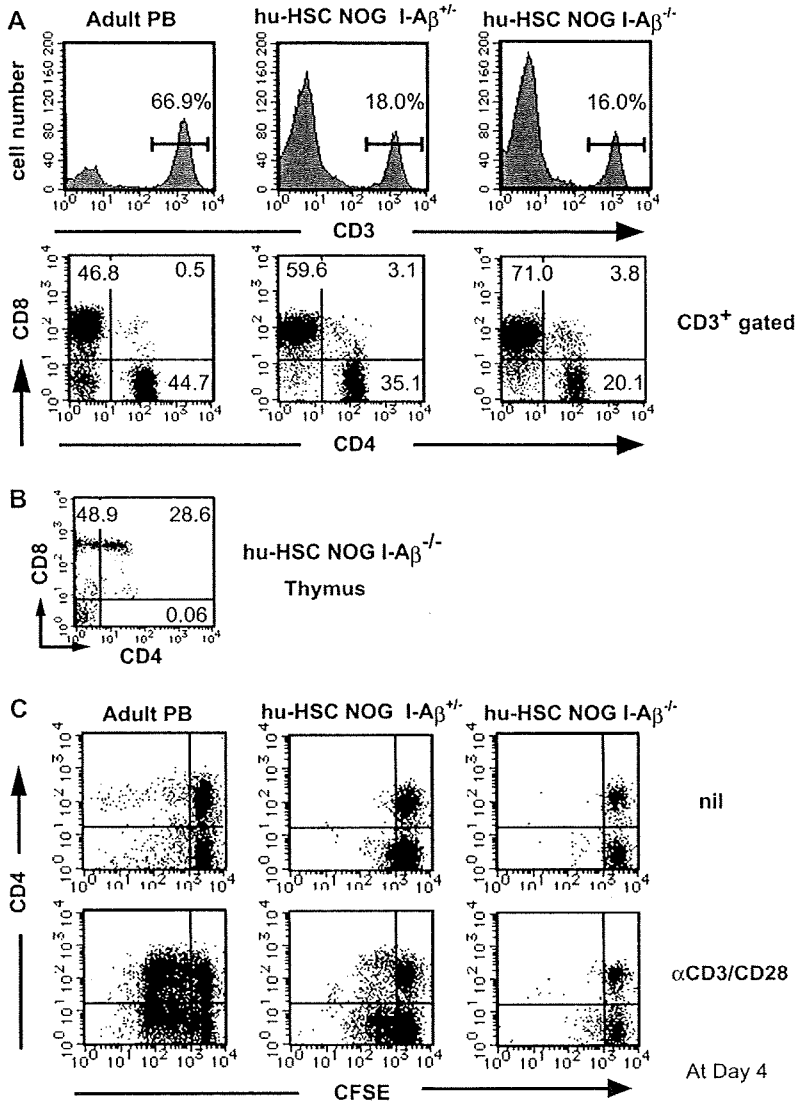

Fig. 9. Analysis of human T cells developed in hu-HSC NOG I-Aβ$^{-/-}$ mice. (A) NOG I-Aβ$^{+/-}$ or NOG I-Aβ$^{-/-}$ mice were reconstituted with human CD34$^+$ stem cells as described in Methods. Adult peripheral blood (PB) or the whole-spleen cells from respective humanized mice (20 weeks after reconstitution) were stained with anti-CD3 antibody (top panel). The CD3-positive cells were further stained with anti-CD4 and CD8 antibodies (bottom panels). A representative staining of four independent experiments is shown. (B) Development of thymocytes in hu-HSC NOG I-Aβ$^{-/-}$ mice. The pooled thymocytes from three NOG I-Aβ$^{-/-}$ mice (20 weeks after reconstitution) were stained with anti-CD4 and CD8 antibodies. (C) Analysis of functions of human CD4$^+$ T cells in the hu-HSC NOG I-Aβ$^{-/-}$ mice *in vitro*. The whole-spleen cells from the hu-HSC NOG I-Aβ$^{+/-}$ or hu-HSC NOG I-Aβ$^{-/-}$ mice (20 weeks after reconstitution) or adult PB were stained with CFSE, subsequently cultured in the presence of anti-CD3 and anti-CD28 antibodies. The cultured cells were recovered on day 4 and stained with anti-CD4 and anti-CD8 antibodies. The intensity of CFSE in CD4$^+$ or CD8$^+$ T cells was examined by FACS. A representative result from three independent experiments is shown.

The function of the 'mature' human IgD$^+$ B cells in hu-HSC NOG mice is reasonable, considering that they had an IgG response *in vitro* and *in vivo*. In contrast, there were at least three major obstacles on the T-cell side. The first was the T cells' high susceptibility to cell death. The second was their unresponsiveness, represented by their low proliferation and low production of IL-2. The third was the poor maintenance of human T cells in the mouse environment. However, several other regulatory mechanisms would be present that could also induce the loss of human T-cell function in the mouse periphery. These functional abnormalities contradict previous reports suggesting that functional human T cells develop in humanized mice, although those studies did not analyze the functions in detail (20, 22, 39, 40).

Our results using hu-HSC (*bcl-2*) NOG mice, in which the thymocytes were reactive while the splenic T cells were not, suggested that although human T cells are positively selected in the mouse thymus, they lose their function mainly in the periphery. Given the normal positive selection of human T cells in the mouse thymus, why are they compromised

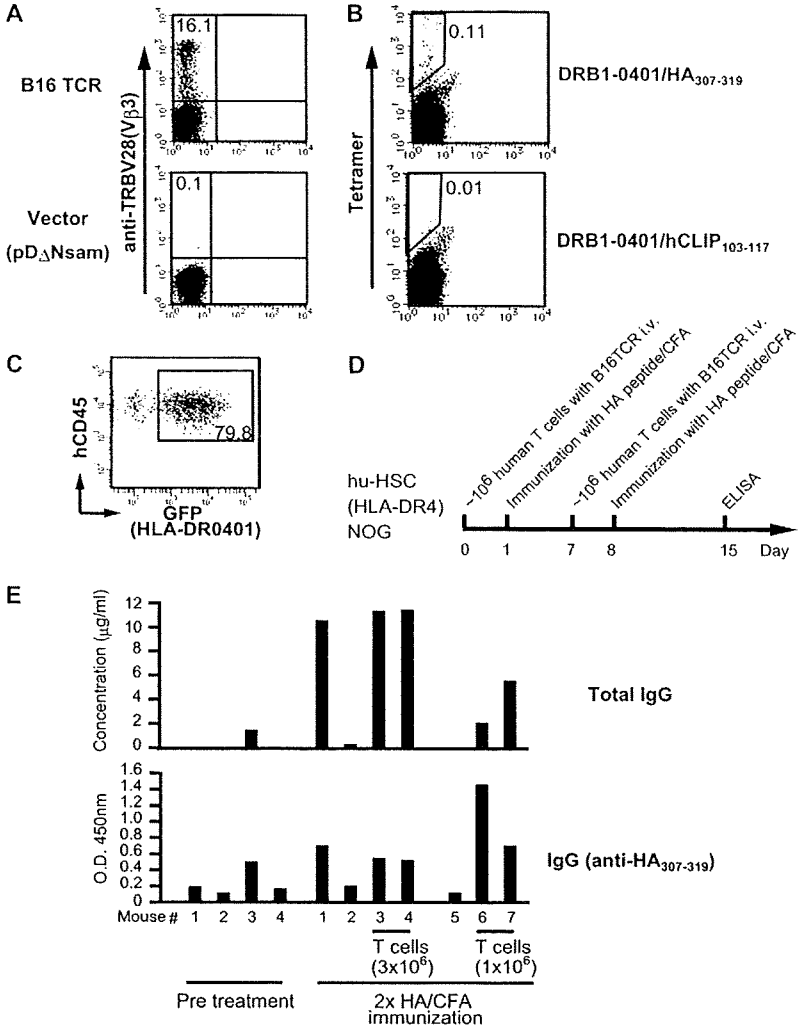

Fig. 10. Induction of IgG in hu-HSC NOG mice. (A) Retroviral delivery of $HA_{307-319}$ peptide-specific TCR (B16) into normal human T cells. Purified human T cells from normal healthy donor were activated *in vitro* as described in Methods. The T cells were subsequently spun infected with retrovirus encoding B16 TCR. The expression of B16 TCR was determined by anti-TRBV28 antibody after 10 days. (B) The frequency of the T cells with B16 TCR was further determined by staining with the specific (middle panels) or irrelevant (right panels) tetramers. (C) Reconstitution of hu-HSC [HLA-DR4 (DRB1*0401)] NOG mice. The expression of the exogenous *HLA-DRB*0401* gene in peripheral blood cells from hu-HSC [HLA-DR4 (DRB1*0401)] NOG mice was represented by bicistronic GFP from retroviral vector (8 weeks after reconstitution, $n = 6$). (D) The schema of experiments for inducing IgG in the hu-HSC [HLA-DR4 (DRB1*0401)] NOG mice upon transfer of B16 TCR-bearing human T cells. (E) Quantification of total IgG or peptide-specific IgG in the hu-HSC [HLA-DR4 (DRB1*0401)] NOG mice. One week after final antigenic challenge, the sera were collected form the mice. Total IgG (left panel) and HA-specific IgG (right panel) were measured by ELISA after 10-fold dilution of the specimens. The results from three or four different mice in each group were shown.

in the periphery? It has been controversial whether the mouse MHC on mouse thymic epithelial cells or the HLA molecules on human BM-derived cells are responsible for the thymic selection of human T cells in the hu-HSC NOG mouse. The significant delay of human T-cell development in hu-HSC NOG I-A$\beta^{-/-}$ mice suggests that the I-A on mouse epithelial cells plays a major role in the positive selection, admitting that a small number of human $CD4^+$ T cells could still develop in the absence of I-A. In this setting, there are two possibilities. The first is that human T cells are not subjected to proper negative selection by human molecules that are not present in the mouse thymus. Indeed, structural analyses of the thymus of hu-HSC NOG mice showed incomplete formation of the cortex where negative selection occurs (Supplementary Figure S2, available at *International Immunology* Online) (41). In this situation, human T cells would be inappropriately activated by I-A/human molecule-derived peptide complexes on the mouse antigen-presenting cells without the proper co-stimulations due to the barrier of species, rendering a refractory state. The second possibility is that human B cells induce unresponsiveness in the T cells because they are not professional antigen-presenting cells; that is, there is a xenoreaction to the HLA molecules on B cells by the human T cells selected by mouse MHCs.

The poor development and differentiation of human professional antigen-presenting cell like DCs and macrophages in hu-HSC NOG mice may also support this possibility (Supplementary Figure S3, available at *International Immunology* Online). The induction of the refractory state of the human T cells might be attributed to one or both of these mechanisms. As for the high susceptibility to cell death of the human T cells in hu-HSC NOG mice, a previous report suggested the high turnover of human T cells in humanized mice (42). The proliferation would be attributed, in part, to the lymphopenic situation in mouse environment where the number of human T cells is very low. Under the condition, it is possible that the human T cells in hu-HSC NOG mice become susceptible to FAS-mediated cell death (43).

The involvement of mouse I-A in the induction of the refractory state of human T cells in hu-HSC NOG mice might be tested using the hu-HSC NOG I-A$\beta^{-/-}$ mice because they developed human T cells. However, because these T cells had impaired function, the involvement of I-A remains to be determined. The results in hu-HSC NOG I-A$\beta^{-/-}$ mice might suggest that in the absence of class II on thymic epithelial cells, the positive selection of human T cells was simply incomplete or that other mechanisms were responsible for inducing abnormalities in the T cells besides the two described above. To circumvent these problems, it is necessary to construct environments in which there is no interference from mouse class II and from which a sufficient number of human T cells can still be obtained. One possibility might be to combine NOG I-A$\beta^{-/-}$ mice with BLT technology, in which an organoid consisting of pieces of fetal thymus and liver are implanted into mice with the subsequent transfer of CD34$^+$ stem cells from the same donor (44). As an alternative approach, the total replacement of mouse co-stimulatory molecules (CD80, CD86, ICAM-1, ICAM-3, etc.) and class II molecules with human orthologues might be useful.

The maintenance of human T-cell functions in the mouse environment is also important. Previous reports using hu-PBL NOD/scid mice showed that normal human T cells lose their capacity to be activated at a certain period after transplantation (45). In our study, the human T cells bearing an HA-specific TCR did not show any expansion, even after repeated immunization with the specific peptide. Supplementing the mouse model with human cytokines could be a strategy for keeping the human T cells viable and functional.

We found at least two abnormal aspects of the B-cell population in the hu-HSC NOG mice. One was a blockage of the differentiation of B cells around the transitional stage and the other was the unusual appearance of B-cell precursors in the spleen. Nevertheless, our functional analyses suggested that the differentiation and functions of the B cells were relatively close to normal. Further studies examining the B-cell function *in vivo* (e.g. expansion capacity, affinity maturation and differentiation into memory or plasma cells) must be undertaken, and additional efforts are necessary to achieve the full maturation of human B cells in mice. We believe that the hu-HSC NOG mice could be developed into a good model for studying the mechanisms involved in the proper differentiation of human B cells.

Humanized mice are becoming common tools for studying human immunity and its related diseases (46, 47). Knowledge has been accumulating about the molecular mechanisms that regulate the development and functions of hematopoietic cells in both humans and mice. It will be important to examine this information using improved model systems, for example, by creating various transgenic NOG strains that are supplemented with human cytokines or growth factors. More sophisticated humanized mice, if achieved, would lead to a better understanding of human immunity and the development of effective therapeutic treatments for human diseases involving autoimmunity or human-specific viral infections.

Supplementary data

Supplementary Figures S1–S3 are available at *International Immunology* Online.

Funding

Ministry of Education, Culture, Sports, Science and Technology of Japan and Japan Society for the Promotion of Science to K.S. (19059001) and M.I. (18100005); Takeda Scientific Foundation to T.T.

Acknowledgements

We thank K. Murata and M. Ito for the technical assistance and their secretary jobs. The authors have no financial conflict of interest.

Abbreviations

APC	allophycocyanin
BM	bone marrow
CFSE	carboxyfluorescein succinimidyl ester
CIEA	Central Institute for Experimental Animals
cμ	cytoplasmic μ chain
DC	dendritic cell
EGFP	enhanced green fluorescent protein
GAPDH	glyceraldehyde 3-phosphate dehydrogenase
HSA	human serum albumin
i.p.	intra-peritoneal
IRES	internal ribosomal entry site
i.v.	intravenous
KLH	keyhole limpet hemocyanin
KO	knockout
MACS	magnetic cell sorting
NOG	NOD/shi-scid/γc^{null}
PE	phycoerythrin
PI	propidium iodide
RT	reverse transcription
SAC	*Staphylococcus aureus* cowan
SP	single positive
TCR	T-cell receptor
γc	γ chain

References

1 Grabstein, K. H., Waldschmidt, T. J., Finkelman, F. D. *et al.* 1993. Inhibition of murine B and T lymphopoiesis *in vivo* by an anti-interleukin 7 monoclonal antibody. *J. Exp. Med.* 178:257.
2 Dittel, B. N. and LeBien, T. W. 1995. The growth response to IL-7 during normal human B cell ontogeny is restricted to B-lineage cells expressing CD34. *J. Immunol.* 154:58.
3 Leonard, W. J., Shores, E. W. and Love, P. E. 1995. Role of the common cytokine receptor gamma chain in cytokine signaling and lymphoid development. *Immunol. Rev.* 148:97.

4 Schraven, B. and Kalinke, U. 2008. CD28 superagonists: what makes the difference in humans? *Immunity* 28:591.
5 Shultz, L. D., Ishikawa, F. and Greiner, D. L. 2007. Humanized mice in translational biomedical research. *Nat. Rev. Immunol.* 7:118.
6 Manz, M. G. 2007. Human-hemato-lymphoid-system mice: opportunities and challenges. *Immunity* 26:537.
7 Legrand, N., Weijer, K. and Spits, H. 2006. Experimental models to study development and function of the human immune system *in vivo*. *J. Immunol.* 176:2053.
8 Payne, K. J. and Crooks, G. M. 2007. Immune-cell lineage commitment: translation from mice to humans. *Immunity* 26:674.
9 Macchiarini, F., Manz, M. G., Palucka, A. K. and Shultz, L. D. 2005. Humanized mice: are we there yet? *J. Exp. Med.* 202:1307.
10 Manning, D. D., Reed, N. D. and Shaffer, C. F. 1973. Maintenance of skin xenografts of widely divergent phylogenetic origin of congenitally athymic (nude) mice. *J. Exp. Med.* 138:488.
11 McCune, J. M., Namikawa, R., Kaneshima, H., Shultz, L. D., Lieberman, M. and Weissman, I. L. 1988. The SCID-hu mouse: murine model for the analysis of human hematolymphoid differentiation and function. *Science* 241:1632.
12 Shultz, L. D., Schweitzer, P. A., Christianson, S. W. *et al.* 1995. Multiple defects in innate and adaptive immunologic function in NOD/LtSz-scid mice. *J. Immunol.* 154:180.
13 Pflumio, F., Lapidot, T., Murdoch, B., Patterson, B. and Dick, J. E. 1993. Engraftment of human lymphoid cells into newborn SCID mice leads to graft-versus-host disease. *Int. Immunol.* 5:1509.
14 Huppes, W., De Geus, B., Zurcher, C. and Van Bekkum, D. W. 1992. Acute human vs. mouse graft vs. host disease in normal and immunodeficient mice. *Eur. J. Immunol.* 22:197.
15 Larochelle, A., Vormoor, J., Hanenberg, H. *et al.* 1996. Identification of primitive human hematopoietic cells capable of repopulating NOD/SCID mouse bone marrow: implications for gene therapy. *Nat. Med.* 2:1329.
16 Ito, M., Hiramatsu, H., Kobayashi, K. *et al.* 2002. NOD/SCID/gamma(c)(null) mouse: an excellent recipient mouse model for engraftment of human cells. *Blood* 100:3175.
17 DiSanto, J. P., Muller, W., Guy-Grand, D., Fischer, A. and Rajewsky, K. 1995. Lymphoid development in mice with a targeted deletion of the interleukin 2 receptor gamma chain. *Proc. Natl Acad. Sci. USA* 92:377.
18 Cao, X., Shores, E. W., Hu-Li, J. *et al.* 1995. Defective lymphoid development in mice lacking expression of the common cytokine receptor gamma chain. *Immunity* 2:223.
19 Ohbo, K., Suda, T., Hashiyama, M. *et al.* 1996. Modulation of hematopoiesis in mice with a truncated mutant of the interleukin-2 receptor gamma chain. *Blood* 87:956.
20 Shultz, L. D., Lyons, B. L., Burzenski, L. M. *et al.* 2005. Human lymphoid and myeloid cell development in NOD/LtSz-scid IL2R gamma null mice engrafted with mobilized human hemopoietic stem cells. *J. Immunol.* 174:6477.
21 Ishikawa, F., Yasukawa, M., Lyons, B. *et al.* 2005. Development of functional human blood and immune systems in NOD/SCID/IL2 receptor {gamma} chain(null) mice. *Blood* 106:1565.
22 Traggiai, E., Chicha, L., Mazzucchelli, L. *et al.* 2004. Development of a human adaptive immune system in cord blood cell-transplanted mice. *Science* 304:104.
23 Hiramatsu, H., Nishikomori, R., Heike, T. *et al.* 2003. Complete reconstitution of human lymphocytes from cord blood CD34+ cells using the NOD/SCID/gammacnull mice model. *Blood* 102:873.
24 Matsumura, T., Kametani, Y., Ando, K. *et al.* 2003. Functional CD5+ B cells develop predominantly in the spleen of NOD/SCID/gammac(null) (NOG) mice transplanted either with human umbilical cord blood, bone marrow, or mobilized peripheral blood CD34+ cells. *Exp. Hematol.* 31:789.
25 Baenziger, S., Tussiwand, R., Schlaepfer, E. *et al.* 2006. Disseminated and sustained HIV infection in CD34+ cord blood cell-transplanted Rag2-/-gamma c-/- mice. *Proc. Natl Acad. Sci. USA* 103:15951.
26 Cosgrove, D., Gray, D., Dierich, A. *et al.* 1991. Mice lacking MHC class II molecules. *Cell* 66:1051.
27 Suemizu, H., Yagihashi, C., Mizushima, T. *et al.* 2008. Establishing EGFP congenic mice in a NOD/Shi-scid IL2Rg(null) (NOG) genetic background using a marker-assisted selection protocol (MASP). *Exp. Anim.* 57:471.
28 Tsuganezawa, K., Kiyokawa, N., Matsuo, Y. *et al.* 1998. Flow cytometric diagnosis of the cell lineage and developmental stage of acute lymphoblastic leukemia by novel monoclonal antibodies specific to human pre-B-cell receptor. *Blood* 92:4317.
29 Kaneko, S., Onodera, M., Fujiki, Y., Nagasawa, T. and Nakauchi, H. 2001. Simplified retroviral vector gcsap with murine stem cell virus long terminal repeat allows high and continued expression of enhanced green fluorescent protein by human hematopoietic progenitors engrafted in nonobese diabetic/severe combined immunodeficient mice. *Hum. Gene Ther.* 12:35.
30 Morita, S., Kojima, T. and Kitamura, T. 2000. Plat-E: an efficient and stable system for transient packaging of retroviruses. *Gene Ther.* 7:1063.
31 Gebe, J. A., Novak, E. J., Kwok, W. W., Farr, A. G., Nepom, G. T. and Buckner, J. H. 2001. T cell selection and differential activation on structurally related HLA-DR4 ligands. *J. Immunol.* 167:3250.
32 Simmons, A. and Jantz, K. 2006. Use of a lentivirus/VSV pseudotype virus for highly efficient genetic redirection of human peripheral blood lymphocytes. *Nat. Protoc.* 1:2688.
33 Sims, G. P., Ettinger, R., Shirota, Y., Yarboro, C. H., Illei, G. G. and Lipsky, P. E. 2005. Identification and characterization of circulating human transitional B cells. *Blood* 105:4390.
34 Imamura, R., Miyamoto, T., Yoshimoto, G. *et al.* 2005. Mobilization of human lymphoid progenitors after treatment with granulocyte colony-stimulating factor. *J. Immunol.* 175:2647.
35 Hystad, M. E., Myklebust, J. H., Bo, T. H. *et al.* 2007. Characterization of early stages of human B cell development by gene expression profiling. *J. Immunol.* 179:3662.
36 Leonard, W. J. and Spolski, R. 2005. Interleukin-21: a modulator of lymphoid proliferation, apoptosis and differentiation. *Nat. Rev. Immunol.* 5:688.
37 Ozaki, K., Spolski, R., Ettinger, R. *et al.* 2004. Regulation of B cell differentiation and plasma cell generation by IL-21, a novel inducer of Blimp-1 and Bcl-6. *J. Immunol.* 173:5361.
38 Choi, E. Y., Jung, K. C., Park, H. J. *et al.* 2005. Thymocyte-thymocyte interaction for efficient positive selection and maturation of CD4 T cells. *Immunity* 23:387.
39 Yahata, T., Ando, K., Nakamura, Y. *et al.* 2002. Functional human T lymphocyte development from cord blood CD34+ cells in nonobese diabetic/Shi-scid, IL-2 receptor gamma null mice. *J. Immunol.* 169:204.
40 Saito, Y., Kametani, Y., Hozumi, K. *et al.* 2002. The *in vivo* development of human T cells from CD34(+) cells in the murine thymic environment. *Int. Immunol.* 14:1113.
41 McCaughtry, T. M., Baldwin, T. A., Wilken, M. S. and Hogquist, K. A. 2008. Clonal deletion of thymocytes can occur in the cortex with no involvement of the medulla. *J. Exp. Med.* 205:2575.
42 Legrand, N., Cupedo, T., van Lent, A. U. *et al.* 2006. Transient accumulation of human mature thymocytes and regulatory T cells with CD28 superagonist in "human immune system" Rag2(-/-) gammac(-/-) mice. *Blood* 108:238.
43 Fortner, K. A. and Budd, R. C. 2005. The death receptor Fas (CD95/APO-1) mediates the deletion of T lymphocytes undergoing homeostatic proliferation. *J. Immunol.* 175:4374.
44 Melkus, M. W., Estes, J. D., Padgett-Thomas, A. *et al.* 2006. Humanized mice mount specific adaptive and innate immune responses to EBV and TSST-1. *Nat. Med.* 12:1316.
45 Tary-Lehmann, M., Lehmann, P. V., Schols, D., Roncarolo, M. G. and Saxon, A. 1994. Anti-SCID mouse reactivity shapes the human CD4+ T cell repertoire in hu-PBL-SCID chimeras. *J. Exp. Med.* 180:1817.
46 Yajima, M., Imadome, K., Nakagawa, A. *et al.* 2008. A new humanized mouse model of Epstein-Barr virus infection that reproduces persistent infection, lymphoproliferative disorder, and cell-mediated and humoral immune responses. *J. Infect. Dis.* 198:673.
47 Kumar, P., Ban, H. S., Kim, S. S. *et al.* 2008. T cell-specific siRNA delivery suppresses HIV-1 infection in humanized mice. *Cell* 134:577.

Highly Sensitive Model for Xenogenic GVHD Using Severe Immunodeficient NOG Mice

Ryoji Ito, Ikumi Katano, Kenji Kawai, Hiroshi Hirata, Tomoyuki Ogura, Tsutomu Kamisako, Tomoo Eto, and Mamoru Ito

Background. Several animal models for xenogenic (xeno) graft versus host disease (GVHD) have been developed in immunodeficient mice, such as C.B-17-*scid* and nonobese diabetes (NOD)/severe combined immunodeficiency (SCID), by human peripheral blood mononuclear cell (hPBMC) transplantation. However, these models pose problems because they require sublethal total body irradiation of the mice and a large number of hPBMCs to induce GVHD, and the timing of onset of GVHD is also unstable. The aim of this study is to establish improved murine models of xeno-GVHD using novel immunodeficient NOD/Shi-*scid* IL2rγ^{null} (NOG) mice.

Methods. In three strains of immunodeficient mice, NOG, BALB/cA-RAG2^{null} IL2rγ^{null}, and NOD/SCID mice, GVHD was induced by transplantation of hPBMCs with or without total body irradiation, and the GVHD symptoms in these strains were compared.

Results. After intravenous transplantation of hPBMCs, NOG mice showed early onset of GVHD symptoms and a small number of hPBMCs (2.5×10^6) was sufficient to induce GVHD when compared with BALB/cA-RAG2^{null} IL2rγ^{null} and NOD/SCID mice. In addition, total body irradiation was not always necessary in the present model.

Conclusions. These results indicate that our model using the NOG mouse is a useful tool to investigate GVHD and to develop effective drugs for GVHD.

Keywords: Xeno-GVHD, Immunodeficient mice, Model animals.

(*Transplantation* 2009;87: 1654–1658)

Graft versus host disease (GVHD) is known as a major complication in allogenic bone marrow (BM) transplantation for therapy of several diseases such as acute/chronic leukemia, aplastic anemia, and congenital immunodeficiency, and is characterized by high mortality after onset. In the recipients, severe damage by donor lymphocyte infusion is generally observed in various organs including the liver, skin, lungs, kidneys, and intestine (*1*). However, there is no effective treatment for this disease to date.

Xenograft model animals using immunodeficient mice have been used for medical research on various human diseases. Severe combined immunodeficient mice (C.B-17-*scid*) discovered by Bosma et al. (*2*), lack functional T and B lymphocytes, and thus provided a first model termed "SCID-hu" by reconstitution with human peripheral blood mononuclear cells (hPBMC) or fetal lymphoid tissues in these mice (*3–8*). However, even in C.B-17-*scid* mice, only a low level of human cells was reconstituted because of the remaining host innate immune system. Nonobese diabetes (NOD)/SCID mice that were modified from C.B-17-*scid* mice are better recipients for engraftment of hPBMC than C.B-17-*scid* mice, probably because of reduced levels of natural killer (NK) cell activity and additional deficiencies in innate immunity (*9, 10*). In fact, in vivo depletion of NK cells in C.B-17-*scid* or NOD/SCID mice by treatment with NK cell-specific antibodies (e.g., anti-asialo-GM1, anti-TM-β1, and anti-NK1.1) resulted in significantly higher engraftment rates of reconstituted human cells (*11, 12*). However, these models still have several problems including the need for sublethal total body irradiation, and the large number of hPBMCs required to induce GVHD, and instability in the timing of onset of GVHD symptoms. In addition, intravenous transplantation of hPBMCs into these animals failed to induce GVHD (*13*). In clinical cases, the cell transfer route is actually restricted through veins but not through the peritoneal cavity in the therapy for BM transplantation. In this sense, the possibility of intravenous transplantation of hPBMCs may be an important issue for xeno-GVHD animal models.

Van Rijn et al. (*14*) reported a new model using H-2^d-RAG2^{null} IL2rγ^{null} mice lacking T, B, and NK cells. This model has advantages compared with NOD/SCID mice, including no leaky lymphocytes or lymphoid tumor formation, and higher engraftment of human T cells than in previous xeno-GVHD

This work was supported by a Grant-in-Aid for Scientific Research (S) from the Ministry of Education, Culture, Sports, Science and Technology (MEXT) of Japan.

Departments of Laboratory Animal Research, Animal Resources Management, and Pathology Research, Central Institute for Experimental Animals, Miyamae, Kawasaki, Japan.

Address correspondence to: Ryoji Ito, Med.Sci., Central Institute for Experimental Animals, 1430 Nogawa, Miyamae, Kawasaki 216-0001, Japan.

E-mail: rito@ciea.or.jp

Received 29 December 2008. Revision requested 20 January 2009.

Accepted 9 March 2009.

ISSN 0041-1337/09/8711-1654

DOI: 10.1097/TP.0b013e3181a5cb07

models. However, this model still has disadvantages because a large number of hPBMCs (3×10^7 cells) and total body irradiation are required to induce GVHD.

NOD/Shi-*scid* IL2rγ^{null} (NOG) mice were recently established by introduction of the interleukin (IL)-2rγ-targeted gene of IL-2rγ KO mice (*15*) by nine backcross matings of IL-2rγ KO mice to NOD/SCID mice. They showed an extremely high engraftment rate of transplanted human cells compared with other immunodeficient mice because of their higher immunodeficiency, that is, the lack of T, B, and NK cells, and reduced functions of macrophage and dendritic cells. Therefore, they are known an excellent model of "humanized mice" where human cells are well developed and differentiated after transfer of human cord blood $CD34^+$ cells (*16–18*).

This study reported a novel xeno-GVHD animal model using these NOG mice, in which the model showed earlier onset of GVHD symptoms by intravenous transfer of hPBMCs.

MATERIALS AND METHODS

Mice

NOG (formal name, NOD.Cg-*prkdc*^{scid}*il2rg*^{tm1Sug}/Jic) and BALB/cA-RAG2^{null} IL2rγ^{null} (RAG2^{null} IL2rγ^{null}; formal name, C.Cg-*rag2*^{tm1Fwa}*il2rg*^{tm1Sug}/AJic) mice were bred and maintained under specific pathogen-free conditions in the Central Institute for Experimental Animals. NOD.CB17-*prkdc*^{scid}/ShiJic (NOD/SCID) mice were purchased from CIEA Japan Inc. (Tokyo, Japan). Mice were housed in sterilized cages and fed sterilized food and water. These three strains of immunodeficient mice were used at the age of 8 to 10 weeks. In most experiments, NOG mice were irradiated with 2.5 Gy, whereas RAG2^{null} IL2rγ^{null} and NOD/SCID mice were irradiated with 3.5 Gy using an X-ray system (MBR-1505R, Hitachi Medical Corp., Tokyo, Japan) 1 day before hPBMC transplantation.

All animal experiments were approved by the Institutional Animal Care and Use Committee and were performed in accordance with Central Institute for Experimental Animal guidelines.

Transplantation of hPBMCs

Human peripheral blood (PB) was obtained from healthy volunteers with their consent and hPBMCs were isolated by a Ficoll-Hypaque (GE Healthcare UK Ltd., England) density centrifugation and washed in phosphate-buffered saline (PBS). Cells were resuspended in PBS and injected through the peritoneal cavity or tail vein into the irradiated or nonirradiated mice. Body weights of all mice were obtained at twice weekly.

Flow Cytometry

PB and spleens were obtained from mice transplanted with hPBMCs and were prepared as single-cell suspensions. Cells were incubated for 30 min at 4°C under protection from light with a mixture of appropriate fluorescently labeled monoclonal antibodies. After washing with PBS containing 1% fetal calf serum, the cells were suspended in propidium iodide solution (Becton Dickinson, BD Biosciences, San José, CA), followed by multicolor flow cytometry with FACS Canto (Becton Dickinson) and analysis by FACS Diva software (Becton Dickinson). The engraftment rates of human cells were expressed as the percentage of human $CD45^+$ cells in total cells. The antibodies used for recognition of the cell surface molecules were anti-human CD45-fluorescein isothiocyanate (FITC, Becton Dickinson) and human CD3-phycoerythrin-Cy7 (PE-Cy7, Beckman Coulter, Inc., CA).

Immunohistochemistry

For immunohistochemistry, liver, lungs, and kidneys from mice transplanted with hPBMCs were fixed with 10% buffered formalin and embedded in paraffin. Sections of 5-μm thick were placed on amino-silane coated glass slides (Matsunami Glass, Osaka, Japan) and were immunostained by the universal immunoenzyme polymer method (Nichirei, Tokyo, Japan). After deparaffinization, sections were incubated with anti-human CD45 monoclonal antibodies (Dako Cytomation, Glostrup, Denmark) overnight at 4°C and were serially incubated with peroxidase-labeled polymer conjugated goat anti-mouse antibody (Histofine Simplestain Max-PO; Nichirei, Tokyo, Japan) for 30 min at room temperature. For color development, these sections were incubated with 0.02% 3,3′-diaminobenzidine (DAB, Dojindo, Kumamoto, Japan) substrate solution containing 0.006% H_2O_2. Immunostained sections were counterstained with hematoxylin for visualization of nuclei.

RESULTS

Induction of GVHD in NOG Mice

To investigate the appropriate route and minimum cell count of hPBMC to induce xeno-GVHD, various numbers of hPBMCs were transferred into irradiated NOG mice by intravenous or intraperitoneal routes (Table 1). On administration of 10×10^6 hPBMCs by the intraperitoneal route, all NOG mice died within 1 month, and 70% (seven of ten) of NOG mice survived for longer than 2 months when 5×10^6 hPBMCs were transplanted. When 5×10^6 or 10×10^6 hPBMCs were transplanted by the intravenous route, all NOG mice died approximately 1 month or 2 weeks earlier than by the intraperitoneal route. In the next experiment, three different counts of hPBMCs (5×10^6, 2.5×10^6, or 1×10^6) were intravenously administered to irradiated three NOG mice each for induction of GVHD (Table 2). NOG mice transplanted with 5×10^6 and 2.5×10^6 hPBMCs died within 1 to 1.5 months after cell transfer. In contrast, all NOG mice transplanted with 1×10^6 cells survived for longer than 3 months. These results demonstrated that the intravenous route was more effective for GVHD induction than the intraperitoneal one, and at least 2.5×10^6 cells are necessary to induce GVHD in NOG mice.

TABLE 1. Comparison of transplantation routes for induction of GVHD in NOG mice

Route of transplantation	Cell numbers of PBMC transferred	Numbers of mice dying from GVHD	Mean days until death
IP	5×10^6	7/10	40.4±9.0
	10×10^6	4/4	23.3±9.7
IV	5×10^6	11/11	26.9±14.6
	10×10^6	8/8	14.5±1.4

IP, intraperitoneal inoculation; IV, intravenous inoculation; GVHD, graft versus host disease; NOG, NOD/Shi-*scid* IL2rγ^{null}; PBMC, peripheral blood mononuclear cell.

TABLE 2. Minimum cell numbers for induction of GVHD in NOG mice

Cell numbers of PBMC transferred	Numbers of mice dying from GVHD	Mean days until death
5×10^6	3/3	34.7±6.7
2.5×10^6	3/3	46.3±14.3
1×10^6	0/3	—

GVHD, graft versus host disease; NOG, NOD/Shi-*scid* IL2rγ^{null}; PBMC, peripheral blood mononuclear cell.

Comparison of Xeno-GVHD Symptoms Among Different Strains of Immunodeficient Mice

To verify the usefulness of NOG mice as a model of xeno-GVHD, we compared the onset and symptoms of xeno-GVHD among three strains of immunodeficient mice, NOG, RAG2^{null} IL2rγ^{null}, and NOD/SCID, that were transplanted with 10×10^6 hPBMCs with or without irradiation (Fig. 1). In transplantation after irradiation, all NOG and RAG2^{null} IL2rγ^{null} mice died at 2 weeks and at 1 to 2 months, respectively, with reduction of body weight in a time dependent manner. In contrast, NOD/SCID mice survived for longer than 2 months without reduced body weight (Fig. 1A). Surprisingly, all NOG mice also died at 1.5 to 2.5 months after transplantation with the same numbers (10×10^6) of hPBMCs without irradiation, but all NOD/SCID and RAG2^{null} IL2rγ^{null} mice survived for more than 3 months (Fig. 1B). These results indicate that NOG mice showed earlier onset of GVHD symptoms and uniformly died when compared with NOD/SCID and RAG2^{null} IL2rγ^{null} mice. In addition, total body irradiation was not necessary for induction of xeno-GVHD only in NOG mice when 10×10^6 hPBMCs were transplanted.

Human Cell Engraftment in Xeno GVHD-Induced Mice

At 2 weeks after transplantation of 5×10^6 hPBMCs through the tail vein of three strains of irradiated immunodeficient mice, we isolated mononuclear cells from PB, BM, and spleen and analyzed engraftment rates of human CD45$^+$ leukocytes by flow cytometry. As shown in Figure 2, the engraftment rates of human CD45$^+$ cells increased more dramatically in PB, BM, and spleens of NOG mice than in those of RAG2^{null} IL2rγ^{null} and NOD/SCID mice. Low rates of engraftment of human CD45$^+$ cells were observed in the spleen from RAG2^{null} IL2rγ^{null} mice but not in NOD/SCID mice. Only a few human CD45$^+$ cells were present in BM and PB of RAG2^{null} IL2rγ^{null} and NOD/SCID mice. The engrafted human CD45$^+$ cells observed in these immunodeficient mice were almost all CD3$^+$ cells (data not shown). These findings suggested that severe GVHD symptoms in NOG mice were caused by higher engraftment of human T cells.

Infiltration of Human Cells in Various Organs

To investigate the infiltration of human lymphocytes into nonlymphoid tissues in xeno GVHD-induced mice, we performed immunohistochemical analysis of the liver, lungs, and kidneys from three strains of irradiated and 5×10^6 hPBMCs transplanted immunodeficient mice using an anti-human CD45 antibody. As seen in Figure 3, remarkably abundant invasion of human CD45$^+$ cells was observed around the veins in the liver, lungs, and kidneys of NOG mice, whereas only a few human CD45 cells were observed in the liver and lungs, and none in the kidneys of RAG2^{null} IL2rγ^{null} and NOD/SCID mice.

DISCUSSION

In present study, we reported a novel model for xeno-GVHD using NOG mice. This model showed significantly rapid onset of GVHD and uniform death after cell transfer when compared with RAG2^{null} IL2rγ^{null} and NOD/SCID models. It also had several advantages over other immunodeficient mice, in that intravenous transplantation was possible, a small number of hPBMCs (2.5×10^6) was sufficient to induce GVHD, and total body irradiation was not always necessary. In previous reports, GVHD was induced effectively by transplantation of PBMCs only by the intraperitoneal route and not by the intravenous route, when xeno GVHD models of SCID or NOD/SCID mice were used. Interestingly, intravenous transplantation could easily induce xeno GVHD in

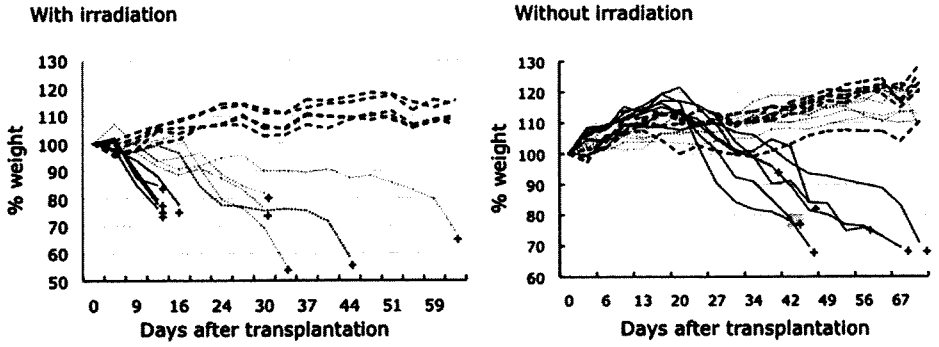

FIGURE 1. Induction of xenogenic graft versus host disease (GVHD) in NOD/Shi-*scid* IL2rγ^{null} (NOG), RAG2^{null} IL2rγ^{null}, and non-obese diabetes (NOD)/severe combined immunodeficiency (SCID) mice. After irradiation (NOG: 2.5 Gy, RAG2^{null} IL2rγ^{null} and NOD/SCID: 3.5 Gy) and after intravenous transplantation of 10×10^6 human peripheral blood mononuclear cells, all mice were weighed twice weekly. All NOG mice died from GVHD with (*left*; n=5) or without (*right*; n=7) irradiation earlier than other immunodeficient mice. All irradiated RAG2^{null} IL2rγ^{null} mice (n=5) died after 1 to 2 months, whereas all nonirradiated mice (n=7) survived for more than 2 months. NOD/SCID mice with or without irradiation (n=5 or n=7) did not die for more than 2 months. Three different *lines* indicate NOG (*solid lines*), RAG2^{null} IL2rγ^{null} (*dotted lines*) and NOD/SCID (*bold dotted lines*); + indicates death of the mouse, and % weight shows weight change percentage from the initial weight.

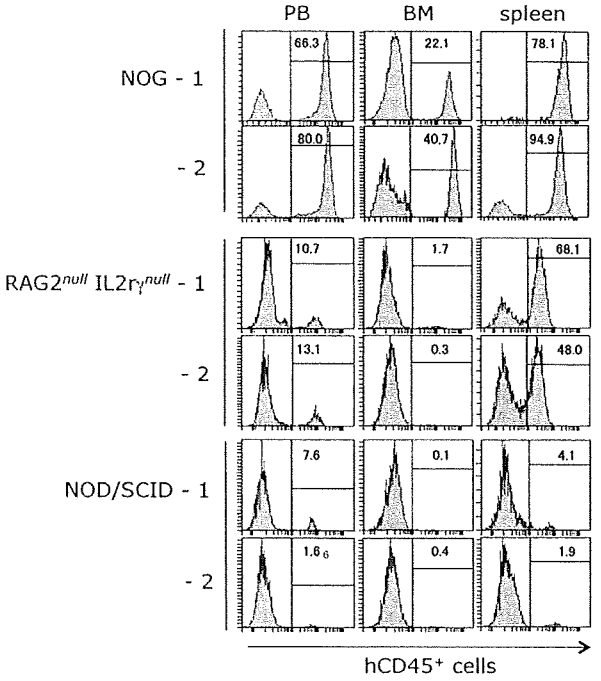

FIGURE 2. Engraftment of human cells in xenogenic graft versus host disease-induced mice. Two weeks after intravenous transplantation of 5×10^6 human peripheral blood mononuclear cells, NOD/Shi-*scid* IL2rγ^{null} (NOG), RAG2^{null} IL2rγ^{null}, and non-obese diabetes (NOD)/severe combined immunodeficiency (SCID) mice were analyzed to determine the rates of human CD45$^+$ cells in peripheral blood, bone marrow, and spleen by flow cytometry as described in Materials and Methods. The histogram shows percentage of human CD45$^+$ cells in total cells and gated living cells by propidium iodide. Results for two typical mice in each strain are shown.

NOG mice. Transplanted hPBMCs were found in the lungs only in the early stage and later became undetectable in C.B-17-*scid* mice injected intravenously, resulting in no GVHD symptoms (*13*). This finding suggests that transplanted hPBMCs may be trapped and rejected in the lungs on intravenous administration.

In our previous studies, NOG mice showed several defects of innate immunity, namely (1) complete lack of NK cells, (2) impaired production of IL-1α by macrophages, and (3) no production of interferon-γ by dendritic cells when compared with NOD/SCID or anti-asialo-GM1-treated NOD/SCID mice (*17*). These results suggest that the main cause of failed engraftment after intravenous injection of hPBMCs into NOD/SCID mice may be innate immunity remaining in the lungs, liver, and other organs.

The composition of mouse immune cells is considered similar in NOG and RAG2^{null} IL2rγ^{null} mice because of the deficiency in T, B, and NK cells in both mice. However, RAG2^{null} IL2rγ^{null} mice showed lower xeno-GVHD sensitivity at the onset of symptoms than NOG mice with or without irradiation. Van Rijn et al. (*14*) reported a xeno GVHD model by intravenous transfer in H-2^d-RAG2^{null} IL2rγ^{null} mice. In their model, chlodronate containing liposomes were used for in vivo depletion of mouse macrophages in liver and spleen before GVHD induction. They showed earlier development of xeno GVHD and higher engraftment of hPBMCs than nontreated H-2^d-RAG2^{null} IL2rγ^{null} mice. Furthermore, Shultz and coworkers (*10*) compared innate immunity among several congenic strains of SCID mice including those of NOD background. They reported that serum hemolytic complement activity in C.B-17- SCID and C57BL/6-SCID mice was elevated when compared with NOD/SCID. We also confirmed a lack of complement activity in NOG mice derived from the NOD background (data not shown). Therefore, these findings suggest that the difference in susceptibility to GVHD between NOG and RAG2^{null} IL2rγ^{null} mice might result from reduction of macrophage function and complement activity in NOG mice.

Fluorescence activated cell sorting analysis revealed a higher engraftment level of human CD45$^+$ cells in NOG mice than in both RAG2^{null} IL2rγ^{null} and NOD/SCID mice. High ratios of human CD45$^+$ cells were also observed in the spleen and PB (60%–90%), but lower ratios in BM (20%–40%).

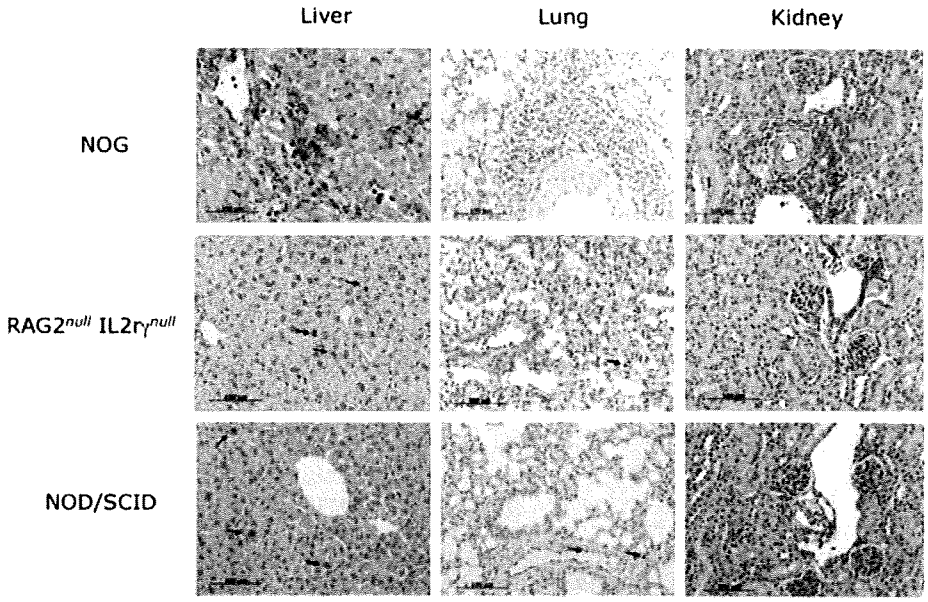

FIGURE 3. Immunohistochemistry in organs from xenogenic graft versus host disease-induced mice. Liver, lungs, and kidneys were obtained from NOD/Shi-*scid* IL2rγ^{null} (NOG), RAG2^{null} IL2rγ^{nul}, and non-obese diabetes (NOD)/severe combined immunodeficiency (SCID) mice intravenously transplanted with 5×10^6 human peripheral blood mononuclear cells at 2 weeks after transplantation. The sections were stained with anti-human CD45 antibody. 3,3′-diaminobenzidine (DAB) substrate was used for color development, and nuclear staining was performed by hematoxylin. *Red arrow* shows human CD45$^+$ cells; magnification ×20.

These distributions of human CD45$^+$ cells in the organs were similar to those in xeno-GVHD as seen in previously reported SCID mouse models (*5, 6, 19*).

The pathophysiology of allogenic GVHD has been described in patients (*20–22*). HLA-mismatched donor-derived T cells are expanded and differentiated to effector cells by recipient and donor derived antigen-presenting cells. Subsequently, the activated donor T cells acquire cytotoxicity that leads to damage in target tissues by the Fas-FasL cascade, perforin/granzyme B-mediated cell attacks, and production of additional inflammatory cytokines, resulting multiple organ failure (*23–25*). Liver, gut, and skin are well known as the target tissues in human or mouse allogenic GVHD. However, the level of lymphocyte infiltration in gut and skin was lower in xeno GVHD models, and it was shown that many cells infiltrated the spleen, lungs, liver, and kidneys (*14*). Similar results were obtained in our model (Fig. 3). Many invading human lymphocytes were found in the liver, lungs, and kidneys but not in skin and gut of 5×10^6 hPBMC-transplanted NOG mice. These findings suggest that the typical histology of the GVHD-targeted tissues may be different between allogenic and xenogenic models. Targeted tissues in allogenic and xenogenic GVHD require further analysis.

The host immune system in patients with GVHD may be still partially active, unlike in the xeno GVHD model in which severely immunodeficient mice were used. This makes it difficult to investigate the actual mechanisms of how donor T cells are activated or suppressed by host-derived antigen-presenting cell, cytokines, or other factors in patients with GVHD. On the other hand, xeno GVHD models have an advantage in examination of the direct suppressive effect of therapeutic agents on human donor cells. Actually, several studies reported that GVHD symptoms were prevented by directly suppressing donor T cells, by regulatory T cells (*26*), by suicide gene-expressed donor T cells (*27*), or by treatment with immunosuppressive agents (*28*) in xeno GVHD models. These approaches may be more effective in preclinical trials in xeno GVHD models than in murine allo-GVHD models.

In conclusion, we developed a novel model for xeno GVHD using NOG mice. This is an excellent model because of the application of intravenous injection and comparatively small numbers for GVHD induction. In addition, NOG mice with or without irradiation expressed more severe symptoms of GVHD than RAG2^{null} IL2rγ^{null} and NOD/SCID mice. Therefore, these models are considered to be a useful tool for studying GVHD, and further studies will be need for clinical applications.

ACKNOWLEDGMENTS

The authors thank Miyuki Ida, Masashi Sasaki, and Eri Hayakawa of CIEA for their technical assistance.

REFERENCES

1. Goker H, Haznedaroglu IC, Chao NJ. Acute graft-vs-host disease: Pathobiology and management. *Exp Hematol* 2001; 29: 259.
2. Bosma GC, Custer RP, Bosma MJ. A severe combined immunodeficiency mutation in the mouse. *Nature* 1983; 301: 527.
3. McCune JM, Namikawa R, Kaneshima H, et al. The SCID-hu mouse: Murine model for the analysis of human hematolymphoid differentiation and function. *Science* 1988; 241: 1632.
4. Mosier DE, Gulizia RJ, Baird SM, et al. Transfer of a functional human immune system to mice with severe combined immunodeficiency. *Nature* 1988; 335: 256.
5. Hoffmann-Fezer G, Gall C, Zengerle U, et al. Immunohistology and immunocytology of human T-cell chimerism and graft-versus-host disease in SCID mice. *Blood* 1993; 81: 3440.
6. Tary-Lehmann M, Saxon A, Lehmann PV. The human immune system in hu-PBL-SCID mice. *Immunol Today* 1995; 16: 529.
7. Abedi MR, Christensson B, Islan KB, et al. Immunoglobulin production in severe combined immunodeficient (SCID) mice reconstituted with human peripheral blood mononuclear cells. *Eur J Immunol* 1992; 22: 823.
8. Carballido JM, Namikawa R, Carballido-Perrig N, et al. Generation of primary antigen-specific human T- and B-cell responses in immunocompetent SCID-hu mice. *Nat Med* 2000; 6: 103.
9. Shultz LD, Schweitzer PA, Christianson SW, et al. Multiple defects in innate and adaptive immunologic function in NOD/LtSz-scid mice. *J Immunol* 1995; 154: 180.
10. Greiner DL, Shultz LD, Yates J, et al. Improved engraftment of human spleen cells in NOD/LtSz-scid/scid mice as compared with C.B-17-scid/scid mice. *Am J Pathol* 1995; 146: 888.
11. Sandhu JS, Gorczynski R, Shpitz B, et al. A human model of xenogeneic graft-versus-host disease in SCID mice engrafted with human peripheral blood lymphocytes. *Transplantation* 1995; 60: 179.
12. Tsuchida M, Brown SA, Tutt LM, et al. A model of human anti-T-cell monoclonal antibody therapy in SCID mice engrafted with human peripheral blood lymphocytes. *Clin Transplant* 1997; 11(5 Pt 2): 522.
13. Martino G, Anastasi J, Feng J, et al. The fate of human peripheral blood lymphocytes after transplantation into SCID mice. *Eur J Immunol* 1993; 23: 1023.
14. van Rijn RS, Simonetti ER, Hagenbeek A, et al. A new xenograft model for graft-versus-host disease by intravenous transfer of human peripheral blood mononuclear cells in RAG2$^{-/-}$ $\gamma c^{-/-}$ double-mutant mice. *Blood* 2003; 102: 2522.
15. Ohbo K, Suda T, Hashiyama M, et al. Modulation of hematopoiesis in mice with a truncated mutant of the interleukin-2 receptor gamma chain. *Blood* 1996; 87: 956.
16. Hiramatsu H, Nishikomori R, Heike T, et al. Complete reconstitution of human lymphocytes from cord blood CD34$^+$ cells using the NOD/SCID/gammacnull mice model. *Blood* 2003; 102: 873.
17. Ito M, Hiramatsu H, Kobayashi K, et al. NOD/SCID/gamma (c) (null) mouse: An excellent recipient mouse model for engraftment of human cells. *Blood* 2002; 100: 3175.
18. Yahata T, Ando K, Nakamura Y, et al. Functional human T lymphocyte development from cord blood CD34$^+$ cells in nonobese diabetic/Shi-scid, IL-2 receptor gamma null mice. *J Immunol* 2002; 169: 204.
19. Murphy WJ, Bennett M, Anver MR, et al. Human-mouse lymphoid chimeras: Host-vs.-graft and graft-vs.-host reactions. *Eur J Immunol* 1992; 22: 1421.
20. Ferrara JL, Levy R, Chao NJ. Pathophysiologic mechanisms of acute graft-vs.-host disease. *Biol Blood Marrow Transplant* 1999; 5: 347.
21. Hill GR, Ferrara JL. The primacy of the gastrointestinal tract as a target organ of acute graft-versus-host disease: Rationale for the use of cytokine shields in allogeneic bone marrow transplantation. *Blood* 2000; 95: 2754.
22. Jacobsohn DA, Vogelsang GB. Acute graft versus host disease. *Orphanet J Rare Dis* 2007; 2: 35.
23. Ferrara JL, Cooke KR, Pan L, et al. The immunopathophysiology of acute graft-versus-host-disease. *Stem Cells* 1996; 14: 473.
24. Schmaltz C, Alpdogan O, Horndasch KJ, et al. Differential use of Fas ligand and perforin cytotoxic pathways by donor T cells in graft-versus-host disease and graft-versus-leukemia effect. *Blood* 2001; 97: 2886.
25. Schmaltz C, Alpdogan O, Muriglan SJ, et al. Donor T cell-derived TNF is required for graft-versus-host disease and graft-versus-tumor activity after bone marrow transplantation. *Blood* 2003; 101: 2440.
26. Mutis T, van Rijn RS, Simonetti ER, et al. Human regulatory T cells control xenogeneic graft-versus-host disease induced by autologous T cells in RAG2−/−gammac−/− immunodeficient mice. *Clin Cancer Res* 2006; 12: 5520.
27. Bondanza A, Valtolina V, Magnani Z, et al. Suicide gene therapy of graft-versus-host disease induced by central memory human T lymphocytes. *Blood* 2006; 107: 1828.
28. Fast LD, DiLeone G, Cardarelli G, et al. Mirasol PRT treatment of donor white blood cells prevents the development of xenogeneic graft-versus-host disease in Rag2−/−gammac−/− double knockout mice. *Transfusion* 2006; 46: 1553.

Journal of Neuroscience Research 87:307–317 (2009)

Evaluation of Human Fetal Neural Stem/Progenitor Cells as a Source for Cell Replacement Therapy for Neurological Disorders: Properties and Tumorigenicity After Long-Term In Vitro Maintenance

Daisuke Ogawa,[1,2] Yohei Okada,[1,3] Masaya Nakamura,[4] Yonehiro Kanemura,[5] Hirotaka James Okano,[1] Yumi Matsuzaki,[1] Takuya Shimazaki,[1] Mamoru Ito,[6] Eiji Ikeda,[7] Takashi Tamiya,[2] Seigo Nagao,[2] and Hideyuki Okano[1]*

[1]Department of Physiology, School of Medicine, Keio University, Tokyo, Japan
[2]Department of Neurological Surgery, Faculty of Medicine, Kagawa University, Kagawa, Japan
[3]Department of Neurology, Graduate School of Medicine, Nagoya University, Nagoya, Japan
[4]Department of Orthopedic Surgery, School of Medicine, Keio University, Tokyo, Japan
[5]Institute for Clinical Research, Osaka National Hospital, National Hospital Organization, Osaka, Japan
[6]Central Institute for Experimental Animals, Tokyo, Japan
[7]Department of Pathology, School of Medicine, Keio University, Tokyo, Japan

It is expected that human neural stem/progenitor cells (hNS/PCs) will some day be used in cell replacement therapies. However, their availability is limited because of ethical issues, so they have to be expanded to obtain sufficient amounts for clinical application. Moreover, in-vitro-maintained hNS/PCs may have a potential for tumorigenicity that could be manifested after transplantation in vivo. In the present study, we demonstrate the in vitro and in vivo properties of long-term-expanded hNS/PCs, including a 6-month bioluminescence imaging (BLI) study of their in vivo tumorigenicity. hNS/PCs cultured for approximately 250 days in vitro (hNS/PCs-250) exhibited a higher growth rate and greater neurogenic potential than those cultured for approximately 500 days in vitro (hNS/PCs-500), which showed greater gliogenic potential. In vivo, both hNS/PCs-250 and -500 differentiated into neurons and astrocytes 4 weeks after being transplanted into the striatum of immunodeficient mice, and hNS/PCs-250 exhibited better survival than hNS/PCs-500 at this time point. We also found that the grafted hNS/PCs-250 survived stably and differentiated properly into neurons and astrocytes even 6 months after the surgery. Moreover, during the 6-month observation period by BLI, we did not detect any evidence of rapid tumorigenic growth of the grafted hNS/PCs, and neither PCNA/Ki67-positive proliferating cells nor significant malignant invasive features were detected histologically. These findings support the idea that hNS/PCs may represent a nontumorigenic, safe, and appropriate cell source for regenerative therapies for neurological disorders. © 2008 Wiley-Liss, Inc.

Key words: neural stem cell; in vivo optical imaging; long-term cultures; long-term engraftment; immunodeficient mouse

Recent progress in stem cell biology has greatly raised the expectation that cell replacement therapies may be developed for a variety of neurological disorders, such as spinal cord injury and neurodegenerative diseases, by using human fetal neural stem/progenitor cells (hNS/PCs) (Reynolds and Weiss, 1992; Svendsen et al., 1998; Carpenter et al., 1999; Uchida et al., 2000; Caldwell et al., 2001; Keyoung et al., 2001; Okano, 2002; Jeong et al., 2003; McBride et al., 2004; Cummings et al., 2005; Iwanami et al., 2005). However, the limited availability of human fetal tissues for ethical reasons makes it difficult to obtain large amounts of hNS/PCs. Therefore, for clinical applications, it is important to be able to expand hNS/PCs in vitro in a manner that maintains their multipotency and ability to self-renew.

Additional Supporting Information may be found in the online version of this article.

Contract grant sponsor: Leading Project for Realization of Regenerative Medicine from the Ministry of Education, Culture, Sports, Science and Technology (MEXT) of Japan; Contract grant sponsor: Japan Science and Technology Agency (SORST); Contract grant sponsor: Ministry of Health, Labor, and Welfare (to H.O.); Contract grant sponsor: Research Fellowships for Young Scientists from the Japan Society for the Promotion of Science (to Y.O.); Contract grant sponsor: Grant-in-Aid for 21st Century COE Program from the MEXT (to Keio University).

*Correspondence to: Hideyuki Okano, MD, PhD, Department of Physiology, Keio University School of Medicine, 35 Shinanomachi, Shinjuku-ku, Tokyo 160-8582, Japan. E-mail: hidokano@sc.itc.keio.ac.jp

Received 29 March 2008; Revised 12 June 2008; Accepted 13 June 2008

Published online 28 October 2008 in Wiley InterScience (www.interscience.wiley.com). DOI: 10.1002/jnr.21843

In addition, because of their low proliferation rate, it takes a long time for hNS/PCs to be expanded from a small number of cells to a sufficient population to use in cell replacement therapies. However, previous in vitro studies showed that subjecting hNS/PCs to multiple passages for up to 300 days in vitro (DIV) reduces their growth rate and alters their neurogenic potential (Caldwell et al., 2001; Kanemura et al., 2002; Piao et al., 2006; Wright et al., 2006; Anderson et al., 2007). Neither the proliferative and differentiation properties nor the in vivo dynamics have been reported for hNS/PCs cultured for longer than 300 DIV. Moreover, the long-term in vivo tumorigenicity of grafted hNS/PCs has never been described and is still uncertain.

Here we examined, both in vitro and in vivo, the differentiation and growth properties of hNS/PCs maintained for approximately 250 DIV (hNS/PCs-250) compared with hNS/PCs maintained for a longer period, approximately 500 DIV (hNS/PCs-500). Furthermore, we established a system for evaluating the in vivo tumorigenicity of hNS/PCs, by transplanting them into the striatum of immunodeficient mice and continuously monitoring the transplanted cells by bioluminescence imaging (BLI) in combination with conventional histology. With this system, we successfully monitored grafted cells for approximately 6 months, to evaluate the tumorigenicity of hNS/PCs as a source for cell replacement therapies.

MATERIALS AND METHODS

Cell Culture

Approval to use human fetal neural tissues and neurosphere cultures was obtained from the ethical committees of Keio University and Osaka National Hospital. Tissue procurement procedures were in accordance with the Declaration of Helsinki and in agreement with the ethical guidelines of the Japan Society of Obstetrics and Gynecology and with the ethical guidelines of the Network of European CNS Transplantation and Restoration (NECTAR). Forebrain tissues from a human fetus (8 weeks gestational age) were obtained from a legal abortion carried out at the Osaka National Hospital, with written informed consent obtained from the donor.

hNS/PCs were cultured using the neurosphere method (Reynolds and Weiss, 1992; Svendsen et al., 1998; Keyoung et al., 2001; Kanemura et al., 2002). The growth medium was a defined DMEM/F-12 (1:1)-based medium (Sigma, St. Louis, MO) supplemented with human recombinant (hr-) epidermal growth factor (20 ng/ml; PeproTech EC Inc., London, United Kingdom), hr-fibroblast growth factor 2 (20 ng/ml; PeproTech EC Inc.), hr-leukemia inhibitory factor (10 ng/ml; Chemicon, Temecula, CA), heparin (5 1g/ml; Sigma), B27 supplement (Invitrogen, Carlsbad, CA), and L-glutamine (200 mM; Invitrogen). Half of the culture medium was replaced with fresh growth medium every week. Neurospheres were passaged every 14 days by dissociating them into single cells using TrypLE select (Invitrogen). Viable cells (2 3 10^6 cells/15 ml) were seeded into 50% fresh growth medium plus 50% neurosphere-conditioned medium in uncoated T75 culture flasks and incubated at 378C in 5% CO_2-95% air. hNS/PCs-250 represent neurospheres passaged 20–25 times; 244–314 DIV; mean 287.3 6 24.2 DIV. hNS/PCs-500 represent neurospheres passaged 36–40 times; 476–526 DIV; mean 503.0 6 18.8 DIV (mean 6 SD).

To induce differentiation, the dissociated hNS/PCs were plated on poly-L-lysine (PLL)-coated coverslips and cultured in the DMEM/F-12/B27 without growth factors (Svendsen et al., 1998; Carpenter et al., 1999; Vescovi et al., 1999) for 7 days. On day 7, the cells were fixed in 4% paraformaldehyde (PFA) for 15 min and processed for immunocytochemical analysis.

Growth Assay

To measure the number of viable cells, the total ATP content was measured by ATP assay using the CellTiter-Glo Luminescent Cell Viability Assay (Promega, Madison, WI; Crouch et al., 1993; Petty et al., 1995). Single-cell suspensions were prepared from neurospheres by enzymatic dissociation with TrypLE select. The number of viable cells in the single-cell suspensions was determined by cell counting using trypan blue dye exclusion. To create a standard curve, 100-11 single-cell suspensions of known densities (1 3 10^5, 2 3 10^5, 4 3 10^5, and 8 3 10^5 cells/ml) were subjected to the ATP assay.

To assay the growth of hNS/PCs-250 and -500, single-cell suspensions from each neurosphere were plated in a 96-well plate (5 3 10^3 cells/100 11). The cell number plated in each well on day 0 was equalized according to the ATP measurement, and the subsequent measurements were normalized to the value on day 0 (day 0 5 1, relative growth rate to day 0). Fresh medium (20 11) was added every 4 days. The ATP assay was performed on days 0 (3 hr after plating), 2, 4, 7, and 11, by adding 100 11 of CellTiter-Glo Reagent to each well adjusted to 100 11 in advance. The luminescence signals were measured by a chemiluminescence detection system (Centro LB960; Berthold Technologies, Bad Wildbad, Germany).

Flow Cytometry

For cell-cycle analysis, the dissociated cells (1 3 10^6 cells) were incubated in 1 ml of hypotonic propidium iodide (PI) solution (1 mg/ml PI, 0.1% citric acid, 0.2% NP-40, 10 mg/ml RNaseA) (Deitch et al., 1982) for 30 min at 48C, followed by a 15-min incubation at 378C to digest the RNA. The fluorescent intensity of the PI was then measured by flow cytometry.

For the cell-surface marker analysis and viability assay, the dissociated cells were incubated in fresh medium at 378C for 1 hr to recover the cell-surface antigens. The cells (1 3 10^7 cells) were suspended in 100 11 Hanks' balanced salt solution (HBSS) and incubated on ice for 30 min with allo phyco cyanin (APC)-conjugated anti-CD133 (Miltenyi Biotec, Tokyo, Japan) and phycoerythrin (PE)-conjugated anti-CD24 (BD Biosciences, Franklin Lakes, NJ), or fluorescvein isothiocyanate (FITC)-conjugated annexin V (BD Biosciences) to detect apoptosis. The cells were washed, resuspended in HBSS containing 1 1g/ml PI, and analyzed by FACS Caliber (BD Biosciences).

Virus Transduction and Bioluminescence Imaging

For the live monitoring of transplanted cells in vivo, we applied bioluminescent imaging (BLI), which has been described previously (Miyoshi et al., 1998; Okada et al., 2005). Human neurospheres and control U87MG cells were transduced by a lentivirus containing the click beetle red luciferase (CBRluc) coding sequence and Venus bicistronic reporter gene connected by an internal ribosomal entry site (IRES) (EF1a-CBRluc-IRES-Venus) (Supp. Info. Fig. 1A). The Venus-positive cells were then collected by a fluorescence-activated cell sorter (FACS) to establish cell lines that stably expressed Venus and CBRluc, as described previously (Masuda et al., 2007) (briefly summarized in Supp. Info. Fig. 1B). We confirmed that the photon counts from these CBRluc-labeled cells were directly proportional to the cell numbers plated in vitro (total cell numbers ranging from 10^2 to 10^6 cells/dish, Supp. Info. Fig. 1C,D). Moreover, the relative number of cells integrated into the host animals after transplantation could be estimated by measuring the photon counts from live animals after an intraperitoneal injection of D-luciferin. We also confirmed that the transduction with the lentivirus did not affect the proliferation or differentiation of hNS/PCs or the survival of the grafted animals (Supp. Info. Fig. 1E,F). A Xenogen-IVIS 100 cooled CCD optical macroscopic imaging system (Caliper Life Sciences, Hopkinton, MA) was used for BLI. All the images were analyzed with Igor (WaveMetrics, Lake Oswego, OR) and Living Image software (Caliper Life Sciences), and the optical signal intensity was expressed as photon counts, in units of photons per second. Each image was displayed as a pseudocolor photon count image superimposed on a gray-scale anatomic image. To quantify the measured luminescence, we defined a specific region of interest (ROI) that covered the area in and around the implanted cells. We used the same ROI for all the animals at all time points to ensure uniform data collection.

Transplantation

All the animal experiments were conducted according to the Guidelines for the Care and Use of Laboratory Animals of the Keio University School of Medicine. Mice were anesthetized and received implants of partially dissociated human neurospheres (2 3 10^6 cells in 4 11 of PBS) stereotactically into the right striatum (2 mm lateral and 1 mm anterior to bregma; depth 3 mm from dura). We used immunodeficient mice to avoid immunological rejection resulting from the xenograft. For short-term analyses of up to 4 weeks, we used NOD/SCID/g_c^{null} (NOG) mice (Central Institute for Experimental Animals, Kanagawa, Japan), which are deficient for the common receptor gamma chain on the severe combined immunodeficiency (NOD/SCID) background (Ito et al., 2002) (n 5 5 for hNS/PCs-250, n 5 4 for hNS/PCs-500, n 5 4 for U87MG). NOD/SCID mice (Charles River, Tokyo, Japan) were used for long-term observation of up to 6 months (n 5 4 for hNS/PC-250, n 5 4 for hNS/PCs-500, n 5 4 for U87MG).

Animals were anesthetized and transcardially perfused with 4% PFA at 4 weeks (1 month), 12 weeks (3 months), and 24 weeks (6 months) after transplantation. The whole brain was removed and postfixed for 8 hr in 4% paraformaldehyde (PFA), soaked overnight in 15% followed by 30% sucrose, and embedded in OCT compound. Coronal sections 14 1m thick were made with a Cryostat (Leica, Wetzlar, Germany) and processed for immunohistochemical analysis.

Immunohistochemistry and Immunocytochemistry

For immunofluorescence analyses, cultured cells or tissue sections were incubated with the following primary antibodies at 48C overnight: anti-human Nestin (1:30,000, rabbit polyclonal) (Nakamura et al., 2003), anti-TuJ-1 (1:500, mouse IgG2b monoclonal) (Sigma), antiglial fiibrillary acidic protein (GFAP) (1:3,000, rabbit polyclonal, Sigma), anti-green fluorescent protein (GFP; 1:25,000, mouse IgG2a, mFX72; a gift from Dr. S. Mitani), anti-Ki67 (1:500, Rb polyclonal IgG) (Novocastra Laboratories, Newcastle Upon Tyne, United Kingdom), antiproliferating cell nuclear antigen (PCNA) (1:1,000; Rb polyclonal IgG) (Oncogene, Boston MA), and anti-human nuclei (1:100, mouse monoclonal IgG1) (Chemicon). After three washes, the samples were incubated with Alexa 488-, 555-, or 647-conjugated secondary antibodies (Invitrogen) for 2 hr at room temperature. Images were obtained by microscopy (Apotome; Carl Zeiss) or confocal laser scanning microscopy (LSM510; Carl Zeiss).

The quantification of different phenotypes in vitro was accomplished by counting the immunolabeled cells on each coverslip. Five separate, randomly chosen fields on each coverslip were counted using a 3 20 objective. The numbers of Nestin-, TuJ-1-, and GFAP-immunoreactive cells are presented as the percentage of total cells, which were stained by Hoechst 33258.

To quantify the Ki67-, PCNA-, and TUNEL-positive cells in tissue sections, the number of immunoreactive cells that were also positively stained by anti-human nuclei were counted in more than five randomly selected fields in each section. These data are presented as the percentage of total cells stained by human antinuclear antigen. Hematoxylin-eosin (HE) staining and HRP-DAB staining were carried out according to standard histological protocols.

Statistical Analysis

Statistical analyses were performed with Student's t-test and Dunn's test. Values are presented as the mean 6 SEM. Significance was accepted at $P < 0.05$.

RESULTS

hNS/PCs Cultured for Long Periods Lost Their Proliferation Ability In Vitro

We first compared the properties of hNS/PCs-250 with those of hNS/PCs-500 in vitro, including the growth rate and differentiation potentials. By ATP assay (Kanemura et al., 2002), hNS/PCs-250 exhibited a significantly higher growth rate than did hNS/PCs-500 (Fig. 1A). Cell-cycle analysis by PI staining showed that the proportion of dividing cells in S/G2/M was 20.5% 6 1.2% for hNS/PCs-250, which was significantly higher than that for hNS/PCs-500 (12.7% 6 0.2%) (n 5 3, $P < 0.01$; Fig. 1B). However, there was no

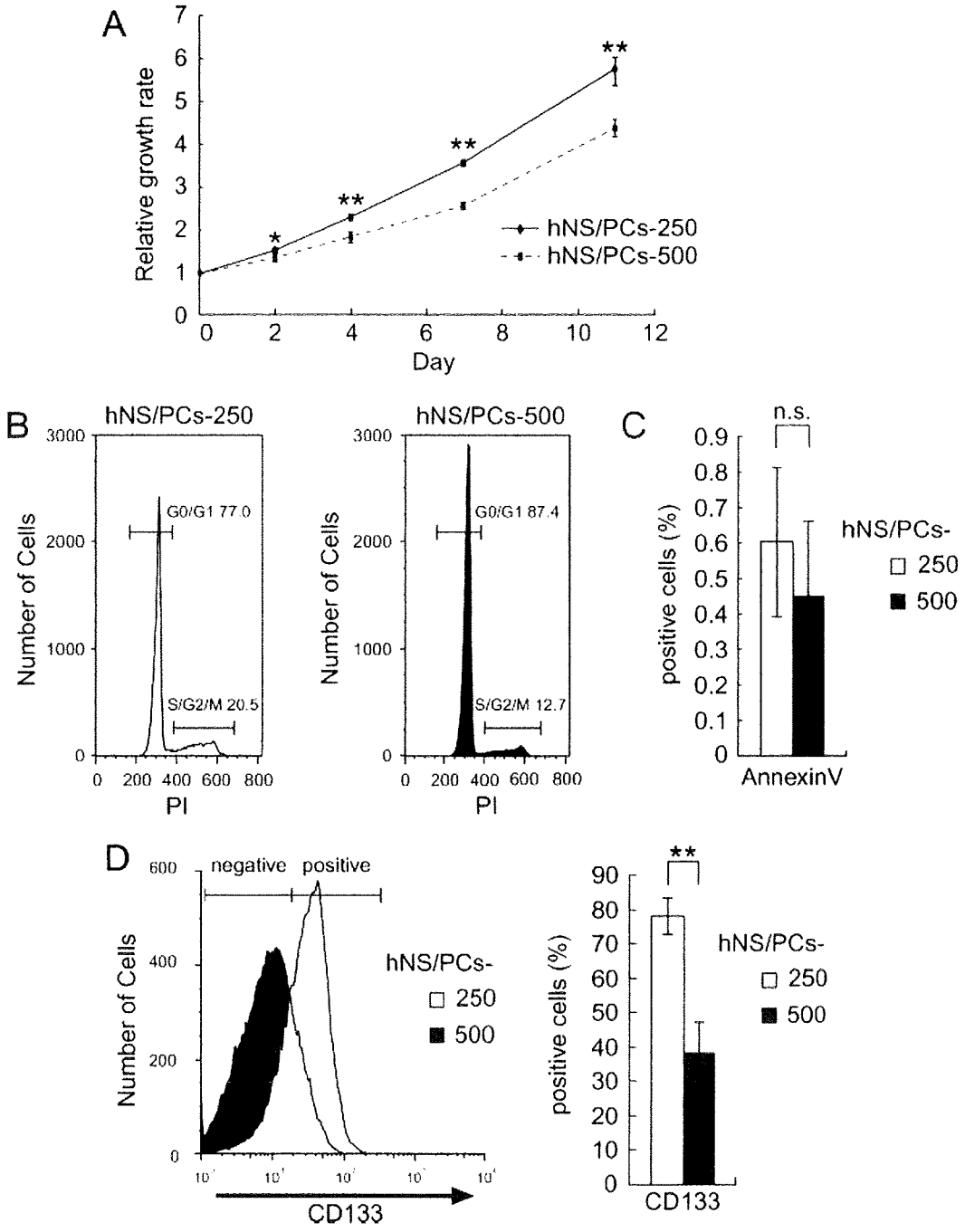

Fig. 1. Comparison of the in vitro properties of hNS/PCs-250 and -500. A: Growth rate of hNS/PCs-250 and -500 examined by ATP assay. hNS/PCs-250 exhibited a significantly higher growth rate than did hNS/PCs-500 during 11 days of culture. B: Cell-cycle analysis by PI staining. The proportion of dividing cells in S/G2/M was significantly higher in hNS/PCs-250 than in -500 ($P < 0.01$). C: Analysis of apoptotic cells by annexin V staining. No significant difference in the proportions of annexin V-positive cells was observed between hNS/PCs-250 and -500. n.s., Not significant ($P > 0.05$). D: Expression of CD133, a marker for undifferentiated hNS/PCs, in hNS/PCs-250 and -500 analyzed by flow cytometry. hNS/PCs-250 contained significantly more $CD133^{1}$ cells than did -500. All data are presented as the mean 6 SEM (n 5 3). *$P < 0.05$; **$P < 0.01$.

significant difference in the proportion of apoptotic cells stained with annexin V between hNS/PCs-250 and -500 (Fig. 1C). These results suggest that the difference in the in vitro growth rate between hNS/PCs-250 and -500 by ATP assay might be attributable to the presence of a differing proportion of proliferating cells, but not of apoptotic cells.

We speculated, based on these results, that there might be a difference in the proportion of undifferentiated hNS/PCs in the neurospheres of hNS/PCs-250 and -500. Therefore, we examined dissociated neurospheres for the expression of cell-type-specific surface markers by flow cytometry. The results indicated that the proportion of $CD133^{1}$ cells, which are known to represent an enriched population of neurosphere-initiating cells (Uchida et al., 2000; Barraud et al., 2007; Panchision et al., 2007), in hNS/PCs-250 was approximately twice that in hNS/PCs-500 (77.9% 6 5.2% and 38.2% 6 8.9% in hNS/PCs-250 and -500, respectively, $P < 0.01$; Fig. 1D), suggesting that the $CD133^{1}$ hNS/PCs in neurospheres may contribute to the higher growth rate seen in hNS/PCs-250 vs. hNS/PCs-500.

hNS/PCs-250 Generated Relatively More Neurons, Whereas hNS/PCs-500 Generated More Astrocytes

We next allowed hNS/PCs-250 and -500 to differentiate on PLL-coated coverglasses without growth factors for 7 days and examined their phenotypes by immunocytochemistry. There was no significant difference in the percentage of Nestin-positive cells between hNS/PCs-250 and -500 (Fig. 2A,B). However, whereas more than 50% of the hNS/PCs-250 differentiated into TuJ-1-positive neurons (54.3% 6 5.5% and 17.6% 6 3.0% in hNS/PCs-250 and -500, respectively, n 5 3, $P < 0.01$), more than 70% of the hNS/PCs-500 differentiated into GFAP-positive astrocytes (23.6% 6 14.7% and 73.5% 6 6.6% in hNS/PCs-250 and -500, respectively, n 5 3, $P < 0.05$). As previously reported, neither hNS/PCs-250 nor hNS/PCs-500 differentiated into CNPase-positive oligodendrocytes in vitro under the same conditions (Iwanami et al., 2005) (data not shown). Consistently with these findings, flow cytometric analyses showed that hNS/PCs-250 contained a greater proportion of $CD24^{1}$ cells, which are proposed to include the cells committed to neuronal lineages (Calaora et al., 1996; Shewan et al., 1996; Doetsch et al., 1999; Nieoullon et al., 2005; Panchision et al., 2007), than did hNS/PCs-500 (73.2% 6 5.4% and 56.1% 6 5.4% in hNS/PCs-250 and -500, respectively, n 5 3, $P < 0.05$; Fig. 2C). Interestingly, most and some of the $CD24^{1}$ cells in the hNS/PCs-250 and -500 were also positive for CD133 (82.2% and 41.8%, respectively; Fig. 2D). Therefore, we also analyzed the $CD133^{2}$ populations and found that the proportion of $CD133^{2}$ cells that were $CD24^{1}$, possibly those representing neuronal progenitors and postmitotic neurons, tended to be higher in the hNS/PCs-250 than in the hNS/PCs-500, although the difference was not statistically significant (61.1% and 51.6% in hNS/PCs-250 and -500, respectively, P 5 0.06; Fig. 2D). Taken together, these findings suggest that hNS/PCs-250 may contain more neurogenic progenitors than do the hNS/PCs-500, which contain more gliogenic progenitors.

hNS/PCs-250 Exhibited Better Survival After Transplantation Into the Striatum of NOG Mice Than Did hNS/PCs-500 by In Vivo Imaging

To assess the survival and differentiation potentials of hNS/PCs in vivo, we stereotactically transplanted hNS/PCs-250, hNS/PCs-500, or U87MG cells, a human glioblastoma cell line, into the right striatum of the intact mouse brain. To avoid immunological rejection of the grafted cells, we used NOG mice (Ito et al., 2002), which are deficient for the interleukin-2 receptor common g chains under the background of severe combined immunodeficiency (NOD/SCID) mice (Shultz et al., 1995).

After transplantation, we observed the survival and growth of the grafted hNS/PCs and U87MG cells for up to 4 weeks (n 5 4 each). For the live monitoring of transplanted cells in vivo, we labeled the hNS/PCs and U87MG with a lentivirus containing the coding sequence for CBRluc and a Venus reporter gene (EF1a-CBRluc-IRES-Venus) (Supp. Info. Fig. 1A) and applied BLI (Okada et al., 2005). The BLI results revealed that the surviving grafted hNS/PCs-250 and -500 decreased sharply, to approximately 20–40% of their original levels 1 week after the transplantation and were maintained thereafter. Four weeks after the transplantation, hNS/PCs-250 showed significantly better survival than did hNS/PCs-500 (12.7% 6 2.4% and 3.8% 6 1.0% of the initial photon counts in hNS/PCs-250 and -500, respectively, n 5 4, $P < 0.01$; Fig. 3A,B). In contrast, the U87MG glioblastoma cells showed logarithmic growth during the 4-week observation period.

Immunohistochemical analyses revealed that both hNS/PCs-250 and hNS/PCs-500 had differentiated into TuJ1-positive neurons and GFAP-positive astrocytes 4 weeks after the transplantation (Fig. 4A). Nestin-positive neural progenitors were also observed in both the hNS/PCs-250 and the hNS/PCs-500 grafts. hNS/PCs-250 contained significantly more Ki67- and PCNA-positive cells than did hNS/PCs-500 (Ki67: 5.1% 6 0.8% and 3.1% 6 0.3%, $P < 0.05$; PCNA: 5.8% 6 0.2% and 4.4% 6 0.3%, in hNS/PCs-250 and -500, respectively, n 5 3, $P < 0.01$; Fig. 4B,C). The percentage of TUNEL-positive apoptotic cells was not significantly different between hNS/PCs-250 and hNS/PCs-500 (0.26% 6 0.05% and 0.37% 6 0.14%, respectively, n 5 3; Fig. 4D,E).

Grafted Neurospheres Survived and Differentiated Into Neurons and Astrocytes In Vivo but Did Not Show Tumorigenicity Even 6 Months After Transplantation

Finally, we evaluated the long-term survival of hNS/PCs and investigated their safety as a cell source

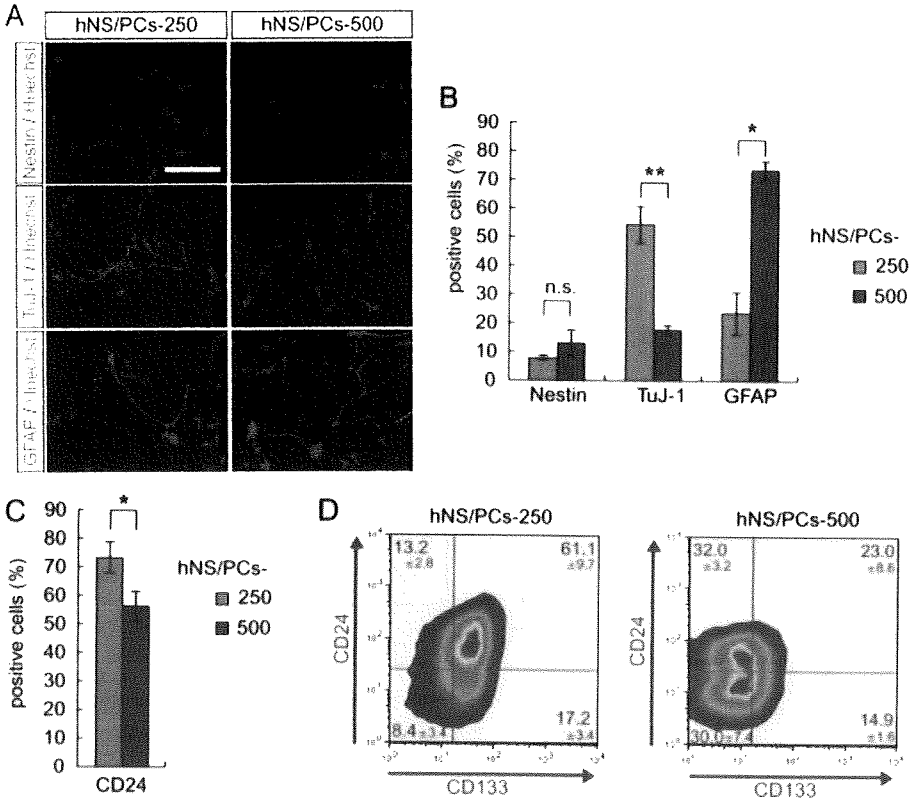

Fig. 2. Altered differentiation potentials between hNS/PCs-250 and -500. A: Immunocytochemical analysis of differentiated hNS/PCs for markers of neural progenitors (Nestin), neurons (TuJ-1), and astrocytes (GFAP). Quantitative analysis is shown in B. Only approximately 10% of the cells in both hNS/PCs-250 and -500 remained positive for Nestin. hNS/PCs-250 differentiated into significantly more TuJ-1-positive neurons than did hNS/PCs-500, whereas hNS/PCs-500 differentiated into significantly more GFAP-positive astrocytes than did hNS/PCs-250. C: Flow cytometric analysis of CD24, which is expressed in populations that include neuronal progenitors and postmitotic neurons. Consistent with the results in B, hNS/PCs-250 contained significantly more CD24-positive cells than did hNS/PCs-500. D: Coexpression of CD133 and CD24 by flow cytometric analysis. Consistently with the results in Figures 1 and 2B, hNS/PCs-250 contained significantly more $CD133^{1}$ cells and $CD24^{1}$ cells than did hNS/PCs-500; n 5 3; means 6 SEM. *P < 0.05; **P < 0.01; n.s., not significant (P > 0.05). Scale bar 5 50 1m.

for transplantation therapy. For long-term observation, we used NOD/SCID mice, which are resistant to stress and infection and therefore show better survival than NOG mice. The results of the short-term experiment revealed that hNS/PCs-500 showed a lower proliferation ability than hNS/PCs-250 in vivo by Ki67 or PCNA immunostaining and a poor survival rate by BLI (only 3.8% 1 month after transplantation even in NOG mice) (Fig. 3A). Thus, for this long-term experiment, we monitored the in vivo tumorigenicity of only the hNS/PCs-250, as the better cell source for cell replacement therapy.

We transplanted hNS/PCs-250 into the right striatum of NOD/SCID mice and observed the survival of the grafted hNS/PCs by BLI for 6 months. The photon count of the luminescence generated by the surviving hNS/PCs was reduced to 12.8% 6 11.0% of the initial photon count at 8 weeks and thereafter maintained its signal for 6 months (10.0% 6 14.0%, n 5 4; Fig. 5A). Notably, no rapid tumorigenic increase of the grafted hNS/PCs was observed within the 6 months following the transplantation. In contrast, control U87MG cells grew rapidly, showing a 419% increase in photon count 4 weeks after transplantation. Among the U87MG-transplanted mice, 75% (three of four) died by 5 weeks and the rest by 6 weeks after transplantation.

To examine the phenotype of the surviving cells derived from the transplanted hNS/PCs, we performed immunohistochemical analyses. Consistent with the findings of BLI, surviving Venus-positive cells were detected 3 months after transplantation (Fig. 5B). Most of them resided at the transplantation site for the entire 6 months and differentiated into TuJ-1-positive neurons and GFAP-positive astrocytes (Fig. 5C). In addition, Nestin-positive neural progenitors persisted even 6 months after the transplantation. However, the grafted hNS/PCs 6 months after transplantation in the long-term animals appeared to have larger nuclei and

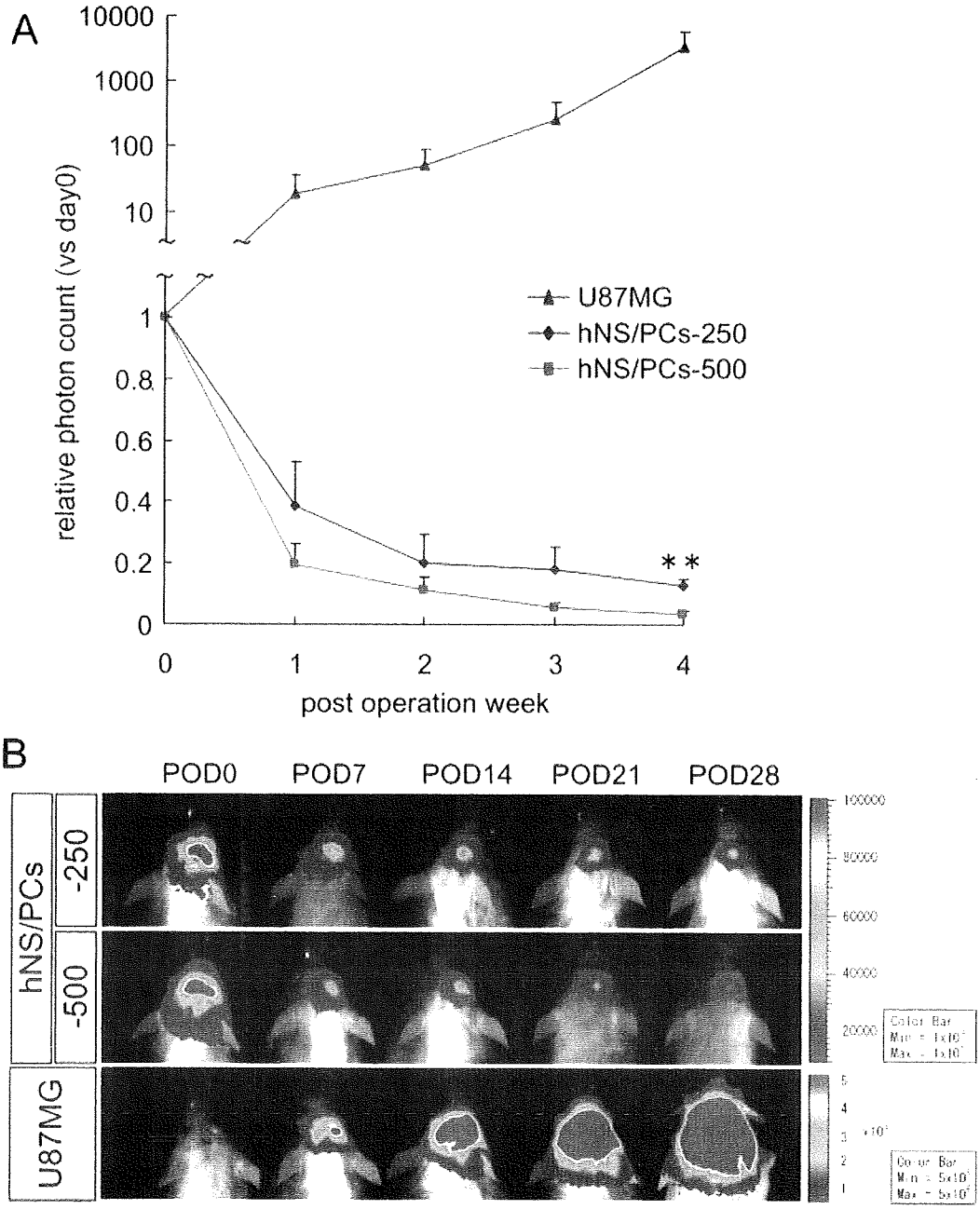

Fig. 3. Bioluminescence imaging of hNS/PCs-250 and -500 transplanted into NOG mice for up to 4 weeks. A: hNS/PCs-250, -500, and human glioblastoma cells (U87MG) were transplanted into the right striatum of NOG mice and observed by BLI for up to 4 weeks. hNS/PCs-250 exhibited significantly better survival and growth than did hNS/PCs-500 4 weeks after transplantation (n 5 4; means 6 SEM). **P < 0.01. B: Representative BLI images of the treated mice.

lower cell densities than those observed 4 weeks after transplantation in the short-term animals (Fig. 5D). Importantly, we did not find any proliferating cells labeled by Ki67 or PCNA 6 months after transplantation (Fig. 5E) nor any obvious evidence of malignant invasive behavior by HE staining (Fig. 5F). Together

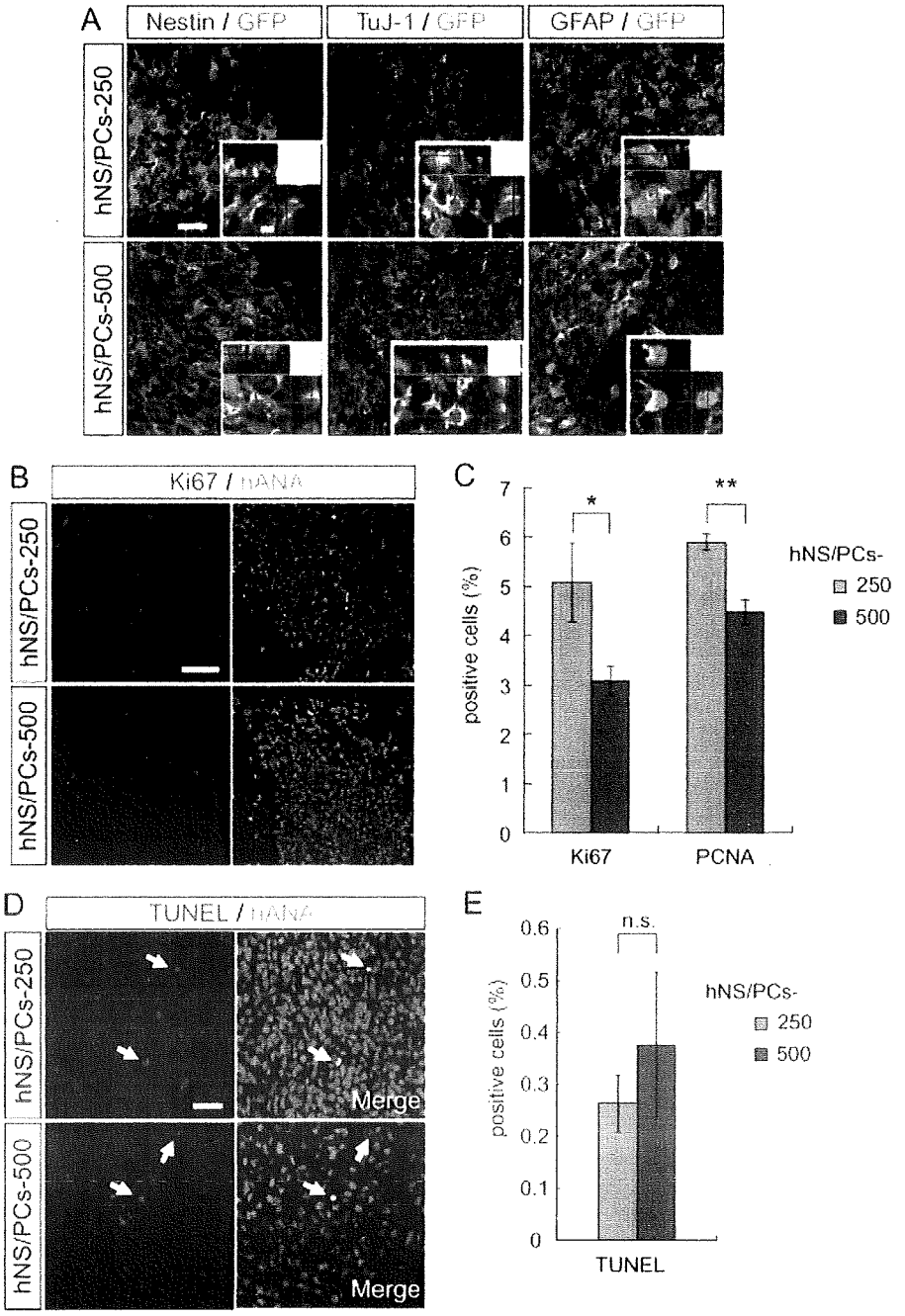

Fig. 4. Both hNS/PCs-250 and -500 appropriately differentiated into neurons and astrocytes in vivo. A: Immunofluorescence analysis of tissue sections 4 weeks after transplantation. Although some of the grafted hNS/PCs-250 and -500 still expressed Nestin, they had also differentiated into TuJ-1-positive neurons and GFAP-positive astrocytes. B: Representative image of Ki67-positive proliferating cells in the hNS/PCs-250 and -500 grafts. C: Quantitative analysis of the proportion of Ki67- and PCNA-positive cells in grafted hNS/PCs-250 and -500 4 weeks after transplantation. hNS/PCs-250 showed a significantly higher proportion of proliferating cells than did hNS/PCs-500. D: Analysis of apoptotic cells by TUNEL staining in grafted hNS/PCs. E: Quantitative analysis of TUNEL-positive cells. No significant difference in the TUNEL-positive apoptotic cells was observed between hNS/PCs-250 and -500. All data are presented as the mean 6 SEM; n 5 3. *P < 0.05; **P < 0.01; n.s., not significant. Scale bars 5 20 1m and 5 1m for low- and high-magnification images, respectively, in A; 50 1m in B; 20 1m in D.